# The Interstellar Medium of Star-Forming Irregular Galaxies: The View with $ISO^1$

Deidre A. Hunter<sup>2</sup> Lowell Observatory, 1400 West Mars Hill Road, Flagstaff, Arizona 86001 USA; dah@lowell.edu

Michael Kaufman

Department of Physics, San Jose State University, San Jose, CA 95192 USA; kaufman@ism.arc.nasa.gov

David J. Hollenbach, Robert H. Rubin NASA/Ames Research Center, MS 245-3, Moffett Field, CA 94035 USA; hollenbach@ism.arc.nasa.gov, rubin@cygnus.arc.nasa.gov

Sangeeta Malhotra

Johns Hopkins University, Charles and 34th Street, Bloomberg Center, Baltimore, MD 21210 USA; san@tarkus.pha.jhu.edu

Daniel A. Dale, James R. Brauher, Nancy A. Silbermann, George Helou, Alessandra Contursi, and Steven D. Lord

IPAC, 100-22, California Institute of Technology, Pasadena, CA 91125 USA; jimby@ipac.caltech.edu, dad@ipac.caltech.edu, nancys@ipac.caltech.edu, gxh@ipac.caltech.edu, contursi@ipac.caltech.edu, lord@ipac.caltech.edu

### ABSTRACT

We present mid-infrared imaging and far-infrared (FIR) spectroscopy of 5 IBm galaxies observed by ISO as part of our larger study of the interstellar medium of galaxies. Most of the irregulars in our sample are very actively forming stars, and one is a starburst system. Thus, most are not typical Im galaxies. The mid-infrared imaging was in a band centered at 6.75  $\mu$ m that is dominated by polycyclic aromatic hydrocarbons (PAHs) and in a band centered at 15  $\mu$ m that is dominated by small dust grains. The spectroscopy of 3 of the galaxies includes [C II] $\lambda$ 158  $\mu$ m and [O I] $\lambda$ 63  $\mu$ m, important coolants of photodissociation regions (PDRs), and [O III] $\lambda$ 88  $\mu$ m and

<sup>&</sup>lt;sup>1</sup>Based on observations made with *ISO*, an ESA project with instruments funded by ESA Member States (especially the PI countries: France, Germany, the Netherlands, and the United Kingdom), and with the participation of ISAS and NASA.

<sup>&</sup>lt;sup>2</sup>Visiting Astronomer, Cerro Tololo Interamerican Observatory, National Optical Astronomy Observatory, which is operated by the Association of Universities in Astronomy, Inc., under cooperative agreement with the National Science Foundation.

 $[N\,\textsc{ii}]\lambda 122~\mu\textsc{m}$ , which come from ionized gas.  $[O\,\textsc{i}]\lambda 145~\mu\textsc{m}$  and  $[O\,\textsc{iii}]\lambda 52~\mu\textsc{m}$  were measured in one galaxy as well. These data are combined with PDR and H II region models to deduce properties of the interstellar medium of these galaxies.

We find a decrease in PAH emission in our irregulars relative to small grain, FIR, and H $\alpha$  emissions for increasing FIR color temperature which we interpret as an increase in the radiation field due to star formation resulting in a decrease in PAH emission. The  $f_{15}/f_{H\alpha}$  ratio is constant for our irregulars, and we suggest that the 15  $\mu$ m emission in these irregulars is being generated by the transient heating of small dust grains by single photon events, possibly Ly $\alpha$  photons trapped in H II regions. The low  $f_{15}/f_{H\alpha}$  ratio, as well as the high  $f_{[CII]}/f_{15}$  ratio, in our irregulars compared to spirals may be due to the lower overall dust content, resulting in fewer dust grains being, on average, near heating sources.

We find that, as in spirals, a large fraction of the [C II] emission comes from PDRs. This is partly a consequence of the high average stellar effective temperatures in these irregulars. However, our irregulars have high [C II] emission relative to FIR, PAH, and small grain emission compared to spirals. If the PAHs that produce the 6.75  $\mu$ m emission and the PAHs that heat the PDR are the same, then the much higher f<sub>[CII]</sub>/f<sub>6.75</sub> ratio in irregulars would require that the PAHs in irregulars produce several times more heat than the PAHs in spirals. Alternatively, the carrier of the 6.75  $\mu$ m feature tracks, but contributes only a part of, the PDR heating, that is due mostly to small grains or other PAHs. In that case, our irregulars would have a higher proportion of the PAHs that heat the PDRs compared to the PAHs that produce the 6.75  $\mu$ m feature.

The high  $f_{[OIII]}/f_{[CII]}$  ratio may indicate a smaller solid angle of optically thick PDRs outside the H II regions compared to spirals. The very high  $L_{[CII]}/L_{CO}$  ratios among our sample of irregulars could be accounted for by a very thick [C II] shell around a tiny CO core in irregulars, and PDR models for one galaxy are consistent with this.

The average densities of the PDRs and far-ultraviolet stellar radiation fields hitting the PDRs are much higher in two of our irregulars than in most normal spirals; the third irregular has properties like those in typical spirals. We deduce the presence of several molecular clouds in each galaxy with masses much larger than typical GMCs.

Subject headings: galaxies: irregular — galaxies: ISM — galaxies: individual (IC 10, IC 4662, NGC 1156, NGC 1569, NGC 2366, NGC 6822) — galaxies: star formation — infrared: galaxies — infrared: ISM: continuum — infrared: ISM: lines and bands

### 1. Introduction

The infrared wavelength region offers a variety of diagnostics of the physical state of the interstellar medium (ISM) in galaxies, and the Infrared Space Observatory (ISO, Kessler et al. 1996) has enabled astronomers to observe many of these infrared features to unprecedented sensitivity levels. Under the US Guaranteed Time project to examine the ISM of normal galaxies, we have used ISO to observe a suite of atomic and ionic fine structure lines and the infrared continuum of a large sample of galaxies (Helou et al. 1996). The 69 galaxies in our sample span the full range of Hubble types from early-type E/S0 galaxies to late-type irregulars. For a list of galaxies in the larger sample see Dale et al. (2000). In this paper we report on the group of irregular galaxies in our sample and how they compare to our larger sample of spiral galaxies. The irregulars are interesting because they are more similar to each other and more different as a group from spirals in, for example, dust column depth and because they are the extreme end of the Hubble sequence of disk galaxies in many galactic properties. However, the reader should keep in mind that the irregulars in our sample are not all typical of the Im class since most are very actively forming stars and one is a starburst. The irregular galaxies in our sample are described in detail in the next section.

The data obtained with ISO for our project include broad-band images of galaxies at 6.75  $\mu$ m and 15  $\mu$ m taken with CAM (Cesarsky et al. 1996a) and fluxes of atomic and ionic fine-structure transitions measured using the Long Wavelength Spectrometer (LWS, Clegg et al. 1996). The mid-infrared CAM images are in the regime where light from red stars is decreasing with wavelength and emission from ISM processes has become dominant. The CAM images at 6.75  $\mu$ m (LW2,  $\Delta\lambda$  of 3.5  $\mu$ m) include major Polycyclic Aromatic Hydrocarbon (PAH) features at 6.2  $\mu$ m, 7.7  $\mu$ m, and 8.6  $\mu$ m (Helou et al. 2000). The CAM images at 15  $\mu$ m (LW3,  $\Delta\lambda$  of 6  $\mu$ m), on the other hand, are most sensitive to thermal emission due to very small grains attaining high temperatures (Dale et al. 2000, Malhotra et al. 2001).

The LWS was used in grating line-mode to obtain emission spectra of primary diagnostics of the ISM. These lines include  $[C_{II}]\lambda 158~\mu m$ ,  $[N_{II}]\lambda 122~\mu m$ ,  $[O_{III}]\lambda 88~\mu m$ , and  $[O_{I}]\lambda 63~\mu m$ . The  $[C_{II}]$  and  $[O_{I}]$  are cooling lines for the atomic gas and probe the conditions in photodissociation regions (PDRs), the warm neutral gas cloud surfaces, which constitute a large fraction of the neutral medium in a galaxy. The  $[N_{II}]$  and  $[O_{III}]$  emission lines probe conditions in the  $H_{II}$  regions. A subset of galaxies, including one irregular, was also observed at  $[O_{I}]\lambda 145~\mu m$  and  $[O_{III}]\lambda 52~\mu m$ . The LWS beam of  $\sim 75''$  diameter included most of the optical galaxy for our distant sample of 60 galaxies and was used to explore different environments within our nearby sample of 9 galaxies. (The "distant" sample is defined as galaxies that are not well resolved with respect to the size of the LWS aperture).

We supplement the ISO data with infrared continuum fluxes measured with the Infrared Astronomical Satellite (IRAS) at 12, 25, 60, and 100  $\mu$ m. We also have optical images that show us what the optical counterparts are to the infrared features seen in the CAM images, provide

B-band luminosities for comparison to the infrared, and show us the amount and locations of current star formation in these galaxies. Below we discuss what is known of the galaxies in our sample, the observations that we use here, the results from the mid-infrared CAM imaging—both in terms of morphology and flux ratios, and the infrared line ratios for the ionized and neutral gas and what they imply about the physical conditions in the PDRs.

### 2. The Galaxies

The irregular galaxies in our sample include NGC 1156, NGC 1569, NGC 2366, NGC 6822, and IC 4662. All of the galaxies that we discuss here are classed as IBm, barred Magellanic-type irregulars, by de Vaucouleurs et al. (1991;  $\equiv$ RC3). Most of the irregulars in our sample are not typical of the Im class since the truly typical Im galaxy is too faint in the far-infrared (FIR) for us to have considered observing with ISO, particularly with the LWS (Hunter et al. 1989, Melisse & Israel 1994). NGC 1156, NGC 1569, and IC 4662 are at the high end of the distribution of surface brightness and star formation activity. NGC 2366 is not, but it contains a supergiant H II region. NGC 6822 is a typical irregular and we did detect it (barely) with CAM but it is not bright enough in the FIR for LWS observations within our time allocation. The galaxies and pertinent global characteristics are given in Table 1. Optical H $\alpha$  images are shown in Figure 1 with V-band image contours superposed.

At an  $M_B$  of -18.0, NGC 1156 is at the high end of the range of luminosities seen in normal, non-interacting irregular galaxies (Hunter 1997), and is about 25% brighter than the Large Magellanic Cloud in the B band. Karachentsev, Musella, & Grimaldi (1996) describe NGC 1156 as "the less disturbed galaxy in the Local Universe," and there are no catalogued galaxy neighbors within 0.7 Mpc and  $\pm 150$  km s<sup>-1</sup>. NGC 1156 has a high rate of star formation and H II regions are crowded over the disk.

NGC 1569 has the highest star formation rate of the sample of 69 irregulars examined by Hunter (1997) as determined from its H $\alpha$  luminosity. It has just undergone a true burst of star formation (Gallagher, Hunter, & Tutukov 1984; Israel & van Driel 1990; Vallenari & Bomans 1996; Greggio et al. 1998), meaning that its recent global star formation rate (SFR) is statistically significantly elevated compared to its average past rate. In addition it contains two luminous super star clusters that are likely young versions of globular clusters (Arp & Sandage 1985; O'Connell, Gallagher, & Hunter 1994), and ionized gas filaments that extend well beyond the main optical body of the galaxy (de Vaucouleurs, de Vaucouleurs, & Pence 1974; Hunter & Gallagher 1990, 1992, 1997; Hunter, Hawley, & Gallagher 1993). The starburst is said to have ended  $\sim$ 4–10 Myrs ago but the presence of H II regions and 5 giant molecular clouds (GMCs) (Taylor et al. 1999) suggests that we can consider star formation as on-going. Virial masses of the molecular clouds suggest that the CO–H<sub>2</sub> conversion factor should be 6.6±1.5 times the Galactic value (Taylor et al. 1999). Stil & Israel (1998) have detected a 7 × 10<sup>6</sup> M $_{\odot}$  H I cloud at 5 kpc from NGC 1569 and the hint of a bridge in H I connecting them. The suggestion is that interaction with this cloud is

responsible for the recent starburst.

NGC 2366, located in the M81 Group of galaxies, is a lower luminosity irregular, having almost the same absolute B magnitude as the Small Magellanic Cloud. It contains the supergiant H II complex NGC 2363 at the southwest end of the bar and labelled in Figure 1. NGC 2363 is nearly twice as bright in H $\alpha$  as the 30 Doradus nebula in the Large Magellanic Cloud and contains a large fraction of the total current star-formation activity of the galaxy (Aparicio et al. 1995, Drissen et al. 2000). However, there is also another large H II complex near NGC 2363 and numerous smaller H II regions scattered along the disk.

NGC 6822 is a low luminosity irregular in the Local Group. It contains a modest population of small H II regions (Killen & Dufour 1982; Hodge, Kennicutt, & Lee 1988; Massey et al. 1995), and a modest star formation activity (Hoessel & Anderson 1986, Hodge et al. 1991, Gallart et al. 1996c). The structure and stellar content of the galaxy have been discussed by Hodge (1977), and the SFR over the past 1 Gyr has been found to be approximately continuous (Marconi et al. 1995, Gallart et al. 1996b, Cohen & Blakeslee 1998). NGC 6822 is one of the few irregulars in which a population of asymptotic giant branch stars has been measured (Gallart et al. 1994).

IC 4662 is the lowest luminosity irregular galaxy in our sample. Nevertheless, it has a SFR per unit area that is only a factor of two lower than that of NGC 1569. The physical characteristics of this galaxy have been studied by Pastoriza & Dottori (1981) and Heydari-Malayeri, Melnick, & Martin (1990). Our optical images show a collection of stars with associated  $\rm H\alpha$  emission that appears to be detached from the main body of the galaxy. It is located 1.5', or 890 pc at IC 4662's distance, to the southeast from the center of the galaxy. Whether this is a very tiny, but separate, companion galaxy, or a very unusually placed OB association we cannot tell. For this paper, we will refer to it as IC 4662-A, and it is labelled as such in Figure 1. In the optical IC 4662 does not look disturbed, as could be the case if it were interacting with a companion, but its SFR is unusually high. In addition there are 3 tiny H II regions located well away from the main body of the galaxy and roughly halfway between IC 4662 and IC 4662-A.

In addition to these 5 irregular galaxies that form part of our distant sample of galaxies, our team has observed IC 10 with ISO as part of our sample of nearby, resolved (with respect to the LWS beam) galaxies. Three positions in IC 10 were observed with the LWS. The ISO LWS observations of IC 10 are the subject of another paper (Lord et al. 2000), and the CAM observations have been discussed by Dale et al. (1999). However, we will call upon those results for comparison here. IC 10 has a B-band luminosity that is comparable to that of NGC 2366 but a current SFR per unit area that is 17 times higher. Massey & Johnson (1998) found that the density of evolved massive stars in the Wolf-Rayet phase is several times higher than that of the Large Magellanic Cloud which is a considerably more luminous galaxy. For this reason, Massey & Armandroff (1995) have suggested that IC 10 too is undergoing a burst of star formation. IC 10 is also known to be unusual in having H I gas that extends about 7 times the optical dimensions of the galaxy (Huchtmeier 1979). It is now known that that extended gas contains a large H I cloud

(Wilcots & Miller 1998), like that near NGC 1569, and which has been suggested is falling into the galaxy causing the current heightened star formation activity (Saito et al. 1992). The [C II]158 emission in IC 10 has also been mapped from NASA's Kuiper Airborne Observatory by Madden et al. (1997), and [CI] at 492 GHz and CO rotational transitions have been observed by Bolatto et al. (2000).

All of the irregular galaxies in our sample are metal-poor compared to spirals, a general characteristic of Im galaxies. The oxygen abundances are given in Table 1. The oxygen abundances  $[12+\log({\rm O/H})]$  range from 8.06 to 8.39 for these galaxies. This corresponds to Z of 0.003 to 0.006, which are 20-40% of solar.

### 3. Observations

### **3.1.** *ISO* **Data**

The observations of irregular galaxies obtained with *ISO* by our team are listed in Table 2. All of the irregular galaxies have been imaged in the mid-infrared through the LW2 and LW3 filters of CAM; NGC 1569 has been observed with additional filters but those observations will not be discussed here (see Lu et al. 2000). The full galaxy sample in our program observed with CAM, the nature of the observations, and the data reduction are discussed by Dale et al. (2000). The CAM frames of each galaxy are combined to produce a final 9" resolution. The field of view of NGC 1156, NGC 1569, and IC 4662 is 4.45', that of IC 10 is 7.25', that of NGC 2366 is 8.2', and that of NGC 6822 is 12.65'. The LW2 and LW3 fluxes, f<sub>6.75</sub> and f<sub>15</sub>, for the irregular galaxies discussed here are given in Table 3. Note that foreground stars and, in the case of NGC 2366, a background galaxy have been removed from the images prior to measuring the fluxes.

To compare the CAM images with  $H\alpha$  and V-band images we needed to determine the coordinate system of all the images. The CAM images were rotated according to the information in the headers so that north would be up and east to the left. For ground-based images we used stars identified on the optical image to determine an astrometric solution for the optical image. When we compared the LW2 and LW3 CAM images with the V-band images, where there are stars in common, we found that the two were offset with respect to each other. Since the pointing accuracy of the CAM images is not expected to be better than 12", we have assumed that the coordinate systems of the CAM images needed minor corrections and offset the LW2 and LW3 images to match the V-band images using the stars in common. The offsets were  $\leq 10$ ".

The irregular galaxies have also been observed in FIR atomic and ionic fine-structure lines. The lines that have been observed are listed in Table 2 and the spectra are shown in Figure 2. The full sample of galaxies observed with the LWS, details concerning the observations and data analysis, and the statistical results for the full sample are given by Malhotra et al. (2001). The emission-line fluxes for the irregular galaxies are given in Table 4. Upper limits are  $3\sigma$ . The [C II]

fluxes of NGC 1156 and NGC 1569 have been corrected for overlying foreground [C II] emission in the Milky Way using observations of a nearby off-galaxy position. The corrections are of order 14%. The IC 10 emission-fluxes have been corrected for the fact that IC 10 is extended with respect to the LWS beam, and that affects the derivation of the surface brightness. The correction factors we used were 0.59 for  $[C II]\lambda 158$ , 0.68 for  $[O III]\lambda 88$ , and 0.84 for  $[O I]\lambda 63$ .

When we compare the irregulars to the rest of the galaxies in our distant galaxy sample, we will delete NGC 4418. It is a Seyfert and does not represent a normal galaxy. In plots we will label the distant galaxy sample minus the irregulars as spirals.

### 3.2. Ground-based and Other Data

Integrated infrared fluxes at 12, 25, 60, and 100  $\mu$ m of these galaxies were measured with IRAS. Those fluxes and the FIR luminosity  $L_{FIR}$  integrated from 40–120  $\mu$ m are given in Table 5. The FIR flux is determined from  $f_{FIR} = 1.26 \times 10^{-14} (2.58 f_{60} + f_{100})$  W m<sup>-2</sup>, where  $f_{60}$  and  $f_{100}$  are the fluxes at 60 and 100  $\mu$ m, respectively, in Jy (Helou et al. 1988). The total infrared flux, TIR, for 3–1100  $\mu$ m is estimated from ISO and IRAS data using the empirical formulation of Dale et al. (2001).

We also obtained optical ground-based images of the irregulars at the Perkins 1.8 m telescope at Lowell Observatory from 1992 to 1995 using various TI  $800\times800$  CCDs. The H $\alpha$  images were obtained through a filter centered at 6566 Å with a FWHM of 32 Å. An off-band image was taken through a filter centered at 6440 Å with a FWHM of 95 Å. The H $\alpha$  image of NGC 2366 was constructed from a mosaic of observations at multiple positions. We observed IC 4662 at the Cerro Tololo Interamerican Observatory (CTIO) on 1999 September 17. We used a SITe 2048×2048 CCD on the 1.5 m telescope with a 75 Å FWHM filter centered at 6600 Å. The off-band filter was a broad-band R filter. NGC 6822 was observed in 1988 with a 0.2 m Takahashi telescope that was bolted to the side of the Hall 1.1 m telescope at Lowell Observatory. Those observations are reported by Gallagher et al. (1991).

The off-band image was shifted, scaled, and subtracted from the H $\alpha$  image to produce an image containing only emission from H II regions. These images are used to trace the current star formation activity. Irregular galaxies contain significantly less dust than spirals. Therefore, we do not expect that the optical H $\alpha$  images have missed significant amounts of star formation (Hunter et al. 1989).

We used both spectral photometric standard stars and H II regions in nearby galaxies to calibrate the H $\alpha$  flux. The H $\alpha$  calibrations took into account the blueshift of the passband with temperatures below 20 C and the different transmissions of the filter at the redshift of the calibrating H II region and the object. We note that the H $\alpha$  flux that we measure for IC 4662 is 58% of that measured by Heydari-Malayeri et al. (1990).

In IC 4662 there are three tiny H II regions to the extreme southeast of the galaxy, two close together and a third more separated from them. The two close together have a combined reddening corrected H $\alpha$  luminosity of  $5.2\times10^{36}$  ergs s<sup>-1</sup>, and the third has a luminosity of  $3.3\times10^{36}$  ergs s<sup>-1</sup>. Thus, these H II regions are comparable to the Orion nebula. IC 4662-A has an H $\alpha$  luminosity of  $2.6\times10^{38}$  ergs s<sup>-1</sup>, 1/22 that of IC 4662 itself and consistent with a large OB association,  $\sim$ 25 O7 stars.

To trace the stars, we use broad-band V images. V-band images of NGC 1156, NGC 1569, and NGC 2366 were obtained by P. Massey with the Kitt Peak National Observatory<sup>3</sup> 4 m telescope and a SITe 2048×2048 CCD from 1997 to 1998. NGC 6822 was observed by C. F. Claver with the 4 m telescope and a SITe 2048×2048 CCD at CTIO in 1996. We obtained V-band images of IC 4662 during our observing run at CTIO in 1999 September.

The abundances and reddening of the ionized gas were measured for individual H<sub>II</sub> regions in NGC 1156 and NGC 2366 using a long-slit spectrograph mounted on the Perkins 1.8 m telescope. Details of the observations and analysis are given by Hunter & Hoffman (1999).

The H $\alpha$  luminosities of the irregulars have been corrected for reddening using total gas  $E(B-V)_g$  given in Table 1. These were determined from Balmer decrements in emission-line spectra. The reddening correction uses the reddening curve of Cardelli et al. (1989). Most stars, however, will not be as extincted as those in H II regions. Therefore, integrated B-band luminosities, taken from RC3, are corrected for reddening using the foreground  $E(B-V)_f$  plus 0.05 magnitude to account for internal reddening of the stars.

Star formation rates are derived from the H $\alpha$  luminosities using a Salpeter stellar initial mass function from 0.1 to 100 M $_{\odot}$  (Hunter & Gallagher 1986). The star formation rates are normalized to the area of the optical galaxy using  $\pi R_{25}^2$ , where  $R_{25}$  in kpc is the radius at a B-band surface brightness of 25 magnitudes arcsec<sup>-2</sup>.

In plots we will include spiral galaxies from the larger distant galaxy sample for comparison. H $\alpha$  fluxes for these galaxies have also been measured from H $\alpha$  images obtained at Lowell Observatory, Palomar Observatory, and Kitt Peak National Observatory. The H $\alpha$  fluxes of the spirals are corrected for reddening assuming a total E(B-V)<sub>g</sub>=E(B-V)<sub>f</sub>+0.8 mag, where E(B-V)<sub>f</sub> is the Milky Way reddening determined by Burstein & Heiles (1984). The 0.8 term is added to account on average for typical reddening of H II regions in spiral galaxies. Their H $\alpha$  luminosities are converted to normalized star formation rates in the same way as was done for the irregulars. Integrated B-band luminosities are taken from RC3 and corrected for reddening using the foreground E(B-V)<sub>f</sub> plus 0.15 magnitude to account for internal reddening of the stars.

<sup>&</sup>lt;sup>3</sup>A division of the National Optical Astronomy Observatory, which is operated by the Association of Universities in Astronomy, Inc., under cooperative agreement with the National Science Foundation.

### 4. Mid-Infrared Imaging

### 4.1. Morphology

In Figure 3 we show the CAM LW2 images of the irregulars in our sample with  $H\alpha$  contours superposed. One can see that to a large degree the  $f_{6,75}$  emission traces H $\alpha$  emission: 1) NGC 1156: In NGC 1156 most of the  $f_{6.75}$  emission is found in two blobs that coincide with the brightest H $\alpha$  peaks. There is also some diffuse  $f_{6.75}$  emission and it is outlined by a lower surface brightness  $H\alpha$  contour. The  $f_{15}$  emission is found entirely from the two brightest  $H\alpha$  peaks. 2) **NGC 1569**: In NGC 1569 the  $f_{6.75}$  and  $f_{15}$  emissions are found in two concentrations at the center of the galaxy where the H $\alpha$  emission is also brightest. In Figure 3 the positions of the 5 GMCs mapped by Taylor et al. (1999) are marked along with the positions of the two superstar clusters. The main peak of  $f_{6.75}$  emission in NGC 1569, the northwestern blob, is resolvable into two peaks itself. The brightest peak to the northwest coincides with the bright HII region there and the 5 molecular clouds are situated around the edges. The fainter peak to the southeast sits immediately to the north of a fainter  $H\alpha$  peak and offset to the south of super star cluster A (the northwestern one of the two). A fainter peak to the northeast of this concentration is associated with an H<sub>II</sub> region that is slightly detached from this H<sub>II</sub> complex. Another much fainter peak well detached to the west is not obviously associated with any H $\alpha$  feature. The second brightest concentration of  $f_{6,75}$  emission, the southeastern blob, is primarily associated with the second brightest H<sub>II</sub> concentration. The faint peak of f<sub>6.75</sub> emission to the extreme southeast, and just to the west of the object labeled as a star, is also not obviously associated with any  $H\alpha$  feature in NGC 1569. 3) NGC 2366: In NGC 2366 most of the mid-infrared emission coincides with the supergiant H<sub>II</sub> region NGC 2363 in the southwestern part of the galaxy. There is a much fainter region of f<sub>6.75</sub> emission to the northeast of that which does not obviously correspond to anything in particular in NGC 2366 in the optical, but it is comparable in brightness to other noise elsewhere in the image beyond the optical galaxy. 4) NGC 6822: In NGC 6822 the mid-infrared emission is found in the direction of 5 H II regions which are identified in Figure 3. There is a bit of diffuse emission towards the center of the galaxy but it is of too low signal-to-noise to measure with any degree of confidence. The fluxes given in Table 3 are the combined fluxes of the H II regions. 5) IC **4662**: In IC 4662 we find the  $f_{6.75}$  emission primarily in two bright concentrations with some low surface brightness diffuse emission around them. These are located near the center of the galaxy. Comparison with the H $\alpha$  image suggests that these two concentrations are also the brightest H II complexes in the galaxy. At 15  $\mu$ m we primarily see the brighter of these three regions. We do not detect the small detached H<sub>II</sub> regions to the southeast or IC 4662-A, further to the south.

This theme of the coincidence of mid-infrared emission and H II regions extends to a large degree to IC 10 as well. There one sees a very bright, amorphous blob in the southeast that coincides with the brightest region of H $\alpha$ . There are also several smaller blobs but without a strong correlation between H $\alpha$  intensity and f<sub>6.75</sub> intensity, and there is some lower surface brightness emission that is not obviously connected with H $\alpha$  emission at all. Then to the northwest of the

brightest region, the H $\alpha$  and 6.75  $\mu$ m emission together trace a partial shell of diameter 470 pc (for a distance to the galaxy of 1 Mpc).

Thus, in our sample of irregulars the mid-infrared emission that we measure is associated with regions of star-formation. This may be an issue of detectability. Irregulars have less dust and, hence, the emission over-all in the infrared is reduced relative to spirals. Furthermore, it is the higher surface brightness regions that will preferentially be detected and the fainter, lower surface brightness emission will be lost. In a study of the mid-infrared surface brightness of several nearby galaxies, including IC 10, Dale et al. (1999) found that variations in dust column density are the primary drivers of infrared surface brightness differences. Therefore, it is reasonable to expect that H II regions and associated gas clouds, which have higher columns of gas and dust compared to the general ISM, will be the places that are easiest to detect.

### 4.2. Flux Ratios

Dale et al. (1999) show that the  $f_{6.75}/f_{15}$  ratio is sensitive to the intensity of heating of the ISM and, hence, is a function of the mid-infrared surface brightness. In regions of intense heating this ratio is  $\leq 1$ , whereas in regions of less intense heating, such as interarm regions in spirals, this ratio is  $\geq 1$ . Furthermore, the ratio  $f_{6.75}/f_{15}$  decreases as the surface brightness rises. In the Milky Way, regions far from H II regions have  $f_{6.75}/f_{15}$  ratios of 1–1.8 (Cesarsky et al. 1996b) whereas in or near H II regions values of order 0.2 are seen (see, for example, Cesarsky et al. 1996b,c; Contursi et al. 1998). The decrease in the  $f_{6.75}/f_{15}$  ratio with star formation activity is most likely due to a combination of PAH destruction in high SFR environments and the increasing contribution of very small grain thermal emission in the LW3 passband. The decrease in PAH features, however, does not necessarily mean physical destruction of the PAH itself. If, for example, only singly ionized PAHs produce the 6.75  $\mu$ m feature (Hudgins et al. 1997), a change in the ionization state of the PAH could decrease the 6.75  $\mu$ m intensity. Similarly, coagulation of PAHs onto larger grains in dense regions could suppress the fluorescence that leads to the 6.75  $\mu$ m emission.

In Table 3 we give the integrated  $f_{6.75}/f_{15}$  ratios for the irregulars as well as the values measured for individual H II regions in these galaxies. One can see that the supergiant H II complex NGC 2363 and, because it is dominated by this H II complex, its galaxy NGC 2366 have the lowest  $f_{6.75}/f_{15}$  ratios, a value of 0.1. Given the large number of hot O stars that have recently formed in NGC 2363 it is not surprising that NGC 2363 has a very low value of  $f_{6.75}/f_{15}$ . The rest of the galaxies, as well as the rest of the H II regions, have higher values of  $f_{6.75}/f_{15}$ , from 0.2–0.6. This range is significantly lower than the  $f_{6.75}/f_{15}$  value of unity typical for quiescent environments, and the values are typical of star-forming regions. The variation in the ratio is presumably due to variations in the intensity of the local stellar radiation field and dust content, although hardness of the radiation field is also a possibility, but it is clear that the mid-infrared emission is being dominated by the dust in or near H II regions in the irregulars.

In Figure 4 we plot the  $f_{6.75}/f_{15}$  ratio against the FIR color temperature ratio  $f_{60}/f_{100}$ , after the figure of Dale et al. (2000), in order to compare the irregulars to the large sample of spirals. The dashed line marks a  $f_{6.75}/f_{15}$  ratio of 1. First, we see that the irregulars in our sample all lie below this line, with values of  $f_{6.75}/f_{15} < 1$ , as we have already discussed. However, it is also true that most of the galaxies in the sample of spirals also have ratios <1. This is due to the fact that the integrated mid-infrared fluxes are dominated by the higher surface brightness regions in the beam, which have low values of  $f_{6.75}/f_{15}$  (Dale et al. 1999); the observations are not as sensitive to the lower surface brightness emission that has a higher  $f_{6.75}/f_{15}$  ratio.

Second, we see that, compared to the spirals, the high infrared-luminosity irregular galaxies in our sample do not have unusual ratios of  $f_{6.75}/f_{15}$ , but they do extend the range to the lowest values; all but one of the irregulars and IC 10 have values at the low end of the range. This is consistent with the mid-infrared emission that we detect in the irregular galaxies being more dominated by star-forming regions than is the case in spirals. We speculate that irregular galaxies with lower star formation rates than those in our sample would show more moderate values of this ratio if they could be detected outside the brightest few H II regions. For example, NGC 6822 is a more typical irregular, but with ISO we have only detected the brightest H II regions.

Third, as Dale et al. (2000) found, we see that the  $f_{6.75}/f_{15}$  ratio drops as the FIR ratio  $f_{60}/f_{100}$  becomes larger, implying warmer large dust grains. One interpretation of this effect is, that as the dust radiating in the FIR becomes warmer, the emission from very small grains at 15  $\mu$ m increases more than the PAH features at 6.75  $\mu$ m. All populations of dust grains should be sensitive to the intensity of the stellar radiation field, but the 15  $\mu$ m emission is most sensitive because it lies on the Wien side of the blackbody spectrum. An alternate possibility is that stronger fields destroy the carriers of the 6.75  $\mu$ m PAH features in irregulars, and we discuss support for this hypothesis below. The exception to this trend is NGC 6822 which has a low value of  $f_{6.75}/f_{15}$  and a low  $f_{60}/f_{100}$ . However, the CAM fluxes in NGC 6822 are quite weak, and the mid-infrared fluxes may be more uncertain than the formal error-bars suggest.

If the mid-infrared ratio  $f_{6.75}/f_{15}$  is sensitive to the stellar radiation field, particularly in and around star-forming regions, one might expect a correlation with the SFR per unit area in a galaxy. That is, the more star formation packed into a given area on average, the more intense the hot star radiation, and the lower the ratio  $f_{6.75}/f_{15}$ . We plot  $f_{6.75}/f_{15}$  against the SFR in Figure 4, where the SFR is a globally averaged value. However, there is no correlation. In fact, four of the irregulars themselves span a range of a factor of 50 in normalized SFR and yet have very similar  $f_{6.75}/f_{15}$  ratios. Most likely, the  $f_{6.75}/f_{15}$  ratio depends on very local conditions (Contursi et al. 2000). The early type stars are only a few parsecs away from the absorbing dust for these ratios, whereas the SFR is averaged over kiloparsec scales. In other words, the SFR per unit area depends on how many star-forming clouds populate a square kiloparsec of galactic disk, whereas the FIR dust temperatures and the  $f_{6.75}/f_{15}$  ratios depend only on how far away the exciting stars lie from the absorbing dust in an individual cloud. There is, therefore, little correlation between the two.

Since the mid-infrared emission spatially traces the H $\alpha$  emission so well in our irregulars, we have considered the ratio of the mid-infrared fluxes to the H $\alpha$  flux,  $f_{6.75}/f_{H\alpha}$  and  $f_{15}/f_{H\alpha}$ , both for galaxies as a whole and for individual H II regions. The integrated ratios are shown for our irregular galaxies, as well as for the spirals, in Figure 5, and are listed in Table 3. The  $f_{6.75}/f_{H\alpha}$  and  $f_{15}/f_{H\alpha}$  ratios depend on a proper correction for extinction at H $\alpha$ . We have used an average internal E(B-V) for the spirals and others might make a different choice (see, for example, Kennicutt 1983). Thus, the spiral  $f_{H\alpha}$  are uncertain by factors of 2–3, but that is still small compared to the trend seen in Figure 5 and small compared to the difference between the bulk of the spirals and the irregulars. The irregular with the lowest and most unusual mid-infrared to H $\alpha$  ratios is NGC 6822, but again we note the possibility of uncertainty in the mid-infrared fluxes in this galaxy.

We see that compared to the spirals, the irregulars in our sample have less mid-infrared emission relative to their H $\alpha$  emission, especially for regions of high FIR color temperature. The  $f_{6.75}/f_{H\alpha}$  ratio for spirals, irregulars, and H II regions varies by a factor of 1000, and the irregulars have ratios at the low end or below those of spirals. There is a little less scatter among the entire sample in  $f_{15}/f_{H\alpha}$  than in  $f_{6.75}/f_{H\alpha}$ . According to Dale et al. (1999), the surface brightness in the mid-infrared is sensitive to both heating intensity and dust column density, although the dust column density usually plays the larger role in the surface brightness differences from galaxy to galaxy. The irregulars generally have a lower dust content than spirals (Hunter et al. 1989) due to their lower metallicity. So, dust column density is likely a factor in why the irregulars have lower ratios with respect to H $\alpha$  than the spirals. However, we note that the PAH emission appears to be more sensitive to this than the small dust grain emission since the irregulars differ from the spirals more in  $f_{6.75}/f_{H\alpha}$  than in  $f_{15}/f_{H\alpha}$ .

Among the irregulars themselves, we see that, except for NGC 6822, the irregulars in our sample with the smallest  $f_{6.75}$  emission per H $\alpha$  emission also have the warmest dust in the FIR whereas there is no difference with  $f_{15}$  emission; our irregulars have very similar  $f_{15}/f_{H\alpha}$  ratios. Since the  $H\alpha$  luminosities of the irregulars in our sample vary by a factor of 10, the constancy of  $f_{15}/f_{H\alpha}$  suggests that the emission from small grains is keeping pace with the H $\alpha$  emission. It seems unlikely that the dust column density is varying among our irregulars in just the right way to compensate for variations in  $H\alpha$  emission. (The  $L_{FIR}/L_B$  ratio varies by only a factor of 3 among our sample of irregulars). Thus, the small grains appear to be reacting to the hot stars that are also ionizing the gas that emits at  $H\alpha$ . In other words, more small grains are heated as more hot stars are formed (but see Bolatto et al. [2000] who argue for the destruction of small dust grains in low metallicity, high ultraviolet radiation environments). In addition, they are heated in such a way that their 15  $\mu$ m flux rises linearly with H $\alpha$ , which tracks the ionizing luminosity of the exciting stars if the H<sub>II</sub> regions are significantly ionization-bounded. In the ionization-bounded regime,  $H\alpha$  essentially "counts ionizing photons" from the stars, and therefore it appears that the 15  $\mu$ m flux is similarly counting exciting photons from the stars. This could occur if the 15  $\mu$ m flux is dominated by the transient heating of small grains by single photons, for example. If

those photons were trapped Ly $\alpha$  photons in the H II regions, then the dust column density is not a factor since the photons scatter until absorbed by dust.

However, if this is the case, then, since the 6.75  $\mu$ m flux from PAHs is excited by single photons as well, the decline in the  $f_{6.75}/f_{15}$  ratio with increasing  $f_{60}/f_{100}$  seen in Figure 4 must be explained with a destruction of the 6.75  $\mu$ m PAH carrier with increasing  $f_{60}/f_{100}$  in irregular galaxies. This appears consistent with the decline in  $f_{6.75}/f_{H\alpha}$  with increasing  $f_{60}/f_{100}$ . While the  $f_{15}/f_{H\alpha}$  ratio is constant among the irregulars, the  $f_{6.75}/f_{H\alpha}$  ratio varies by a factor of 6 if we exclude NGC 6822. In other words, as the H $\alpha$  emission increases, the emission by PAHs in the LW2 passband does not keep pace (see also the UV/ISO comparison of Boselli et al. 1997). For NGC 6822 we are not sufficiently confident of the mid-infrared fluxes to argue that NGC 6822 is truly abnormal. From studies of star-forming regions in the Milky Way, we expect that PAHs are more easily destroyed than small grains in the presence of intense stellar radiation fields (Cesarsky et al. 1996b,c; Contursi et al. 1998) or they are charged in such a way that they do not produce the 6.75  $\mu$ m feature. Thus, we are most likely seeing an increase in star formation intensity causing a decrease in PAH 6.75  $\mu$ m emission. This is given additional credence by Figure 6 which plots the ratios of  $f_{6.75}/f_{FIR}$  and  $f_{15}/f_{FIR}$  against  $f_{60}/f_{100}$ . We see that as the FIR color temperature goes up, the ratio of PAH to FIR emission drops, while the ratio of emission from small dust grains to FIR remains more nearly constant, dropping only slightly. (See Dale et al. 2001 for a more thorough discussion of this relationship).

There is a different trend among the spirals. First, there is a scatter of a factor of 40 in  $f_{15}/f_{H\alpha}$  in the spirals that is much greater than in the irregulars. Second, the  $f_{15}/f_{H\alpha}$  ratio in the spirals increases with increasing FIR color temperature. The higher metallicity and, therefore, higher dust column densities in spirals may mean that the small dust particles responsible for the 15  $\mu$ m flux are on average closer to the OB stars and warmer than in irregulars. The 15  $\mu$ m flux in spirals may not be dominated by single photon transient heating, but by the steady emission of warm grains radiating on the Wien side of the blackbody spectrum (Dale et al. 2001, Helou 2001). The scatter is then caused by different density H II regions that give somewhat different temperature small grains (even for the same  $f_{60}/f_{100}$  which indicates the temperature of larger grains further away). The rise in  $f_{15}/f_{H\alpha}$  with  $f_{60}/f_{100}$  is caused by the increased temperature of the small grains as the large grains get warmer.

In the right panels of Figure 5 we plot the mid-infrared to  $H\alpha$  flux ratios against the FIR to B-band luminosity ratio. The more FIR emission there is relative to optical emission (that is, the more cool, large-grain dust emission there is) the higher the mid-infrared emission is relative to  $H\alpha$  emission for both the PAHs and the small dust grains. The irregulars in our sample follow both of these trends, but sit at the low  $L_{FIR}/L_B$  end of the distribution although, as previously noted, their values are more constant in  $f_{15}/f_{H\alpha}$  than in  $f_{6.75}/f_{H\alpha}$  for their  $L_{FIR}/L_B$ . Thus, in these irregulars, the amount of cold dust emission is related to the emission from PAHs, which is consistent with the premise that dust column densities are important in determining the PAH emission and, possibly, that PAH emission originates in the cooler neutral gas (PDR) and dust

that dominates the FIR dust emission. However, the amount of emission from small dust grains is also related to the amount of total dust emission from larger grains as well as would be expected for a continuous dust population (Giard et al. 1994).

Motivated by Helou et al.'s (2001) observation that the ratio of [C II]158 emission to the emission of PAHs in the LW2 passband is constant in galaxies, we have plotted the ratio of the [C II] emission to the mid-infrared emission against the FIR ratio  $f_{60}/f_{100}$  and the ratio  $L_{FIR}/L_B$  in Figure 7. As Helou et al. found, we see that the  $f_{[CII]}/f_{6.75}$  ratio varies by only a factor of 5 for the spiral galaxies. We see that in our irregulars compared to spirals the [C II] emission is elevated relative to that of the PAH emission by a factor of nearly 3, but that it also stays quite constant as  $f_{60}/f_{100}$  changes.

The modest scatter in  $f_{[CII]}/f_{6.75}$  for a large variation in  $f_{60}/f_{100}$  among spirals is interpreted by Helou et al. (2001) as due to the fact that either the same PAHs which heat the PDR gas also produce the  $f_{6.75}$  emission, or that the ratio of the 6.75  $\mu$ m carrier to the grain or PAH population that dominates the PDR gas heating stays constant. In the irregulars in our sample the former interpretation is hard to understand because the ratio of PDR gas heating to 6.75  $\mu$ m emission is up by a factor of 3. This implies that in irregulars the PAHs which produce the 6.75  $\mu$ m feature and do the heating are quite different from their counterpart PAHs in spirals. This could result from the different processing history and make-up of the ISM in irregulars compared to spirals. In the latter interpretation, the increase in the  $f_{[CII]}/f_{6.75}$  ratio in irregulars could be caused by an increase in the PDR heating population relative to the 6.75  $\mu$ m carrier population (although some [C II] emission comes from H II regions where PAHs may be destroyed). However, this seems inconsistent with observations that show that the relative PAH and dust contents remain the same throughout the Milky Way (Giard et al. 1994) although other studies conclude that PAH fractions vary on small scales (see discussion by Helou et al. 2001).

In Figure 7 we see that for a given  $f_{60}/f_{100}$  the  $f_{[CII]}/f_{15}$  ratio for our irregulars is higher than in spirals and that there is a noisy trend such that the warmer the large dust grains in the FIR, the less [C II] emission per small grain emission. Furthermore, there is no trend of the  $f_{[CII]}/f_{6.75}$  ratio with  $L_{FIR}/L_B$  but a very noisy trend of  $f_{[CII]}/f_{15}$  with  $L_{FIR}/L_B$  (see also Malhotra et al. 2001). The higher  $f_{[CII]}/f_{15}$  at a given  $f_{60}/f_{100}$  may be caused by the lower dust content in irregulars due to their lower metallicity, and that results in the average radiating grain being further away from the OB stars and, hence, cooler on average. Perhaps as well, small dust grains subjected to transient heating by single photons, as we have suggested from the  $f_{15}/f_{H\alpha}$  ratio, are more efficient at radiating at 15  $\mu$ m. The trend with  $f_{60}/f_{100}$  suggests that [C II] increases more slowly with increasing radiation fields than does the 15  $\mu$ m emission. This is consistent with PDR models that show a weak dependence of [C II] with increasing UV fields (Hollenbach, Takahashi, & Tielens 1991). Variations in the incident spectral energy distribution may play a role in variations in the observed ratios as well (Dale et al. 2001).

### 5. Infrared Line Data

Far-infrared emission lines observed with ISO are useful diagnostics of the ISM of galaxies. [C II] $\lambda$ 158  $\mu$ m and [O I] $\lambda$ 63  $\mu$ m are important cooling lines of the neutral atomic medium. [N II] $\lambda$ 122  $\mu$ m, [O III] $\lambda$ 88  $\mu$ m, [N III] $\lambda$ 57  $\mu$ m, and [O III] $\lambda$ 52  $\mu$ m emission come from H II regions. The H II regions contribute to the [C II] $\lambda$ 158  $\mu$ m emission as well. [O III] $\lambda$ 88  $\mu$ m and [O III] $\lambda$ 52  $\mu$ m together provide a measure of the electron density  $n_e$  of the H II region, or more strictly, of the O<sup>++</sup> region. Here we examine the ISO emission line ratios observed for the irregulars NGC 1156, NGC 1569, and IC 4662. The other irregulars included in this study, NGC 2366 and NGC 6822, were not observed with the LWS. The observations refer to integrated emission from a large fraction of the optical galaxy, and thus include the full range of galactic environments. Furthermore, the contributions of the different galactic environments are luminosity-weighted.

### 5.1. The Ionized Gas

5.1.1. 
$$[O III]\lambda 52,88$$
 and  $n_e$ 

The  $f_{[OIII]52}/f_{[OIII]88}$  ratio is sensitive to the electron density of the O<sup>++</sup> regions of H II regions. This ratio is given in Table 4 for NGC 1569 (see also Malhotra et al. 2001). It has also been measured from *ISO* observations for IC 10. From the methodology of Rubin et al. (1994) we find that the O<sup>++</sup> regions covered by the LWS beam in NGC 1569 have an average  $n_e$  of  $\leq 300$  cm<sup>-3</sup>. The emission ratio places  $n_e$  in the low density limit and we can only place an upper limit on  $n_e$ . This value of  $n_e$  is comparable to the values measured for two spirals in our sample (Malhotra et al. 2001). The low values of H II region densities are also consistent with the low ( $\leq 200$  cm<sup>-3</sup>) values observed in giant H II regions in irregulars from the ratios of optical [O II] $\lambda 3726,3729$  lines (see, for example, Hunter & Hoffman 1999). However, the [O II] lines measure the density of the O<sup>+</sup> regions and are more appropriate for the C<sup>+</sup> portions of H II regions that contribute to the observed [C II] emission.

5.1.2. 
$$[OIII]\lambda 88 \ \mu m \ and \ T_{eff}$$

The  $L_{H\alpha}/L_{[OIII]88}$  ratio can be used to estimate the effective temperature of the ionizing stars when the oxygen abundance of the gas is taken into account. We have measured this ratio for NGC 1569 and IC 4662, and the values are given in Table 4. We have combined the observed ratios with the models of Rubin (1985) with a density of 100 cm<sup>-3</sup> and scaled for the oxygen abundances given in Table 1. We use a density of 100 cm<sup>-3</sup> since in the previous section we found  $n_e$  to be in the low density limit ( $n_e \leq 300 \text{ cm}^{-3}$ ). Furthermore, in this regime H $\alpha$  and [O III] emissions have the same functional dependence on  $n_e$ , so the ratio  $L_{H\alpha}L_{[OIII]}$  is not dependent on the density. We examine the resulting  $T_{eff}$  for three model choices of the total nebular Lyman

continuum photons per second. These models are appropriate for H II regions that are smaller than the supergiant regions. Because the LWS beam encompasses a large fraction of the galaxy, these are rough estimates of the average stellar effective temperature.

We find that  $T_{eff}$  in NGC 1569 is about 40,000 K (log g=4.0 model) for all three models with the uncertainty in the measured ratio producing an uncertainty of order 1000 K. This  $T_{eff}$  corresponds to an O6.5V star (Conti & Underhill 1988). The total H $\alpha$  luminosity of NGC 1569 would correspond to the equivalent of 4500 O6.5V stars (Panagia 1973). This large number of O stars is consistent with the recent starburst in that galaxy. It has been suggested that the starburst ended 5–10 Myrs ago (Greggio et al. 1998), 4 Myrs ago (Vallenari & Bomans 1996), and 10 Myrs ago (Israel & van Driel 1990). The hydrogen-burning lifetime of an O6.5 star is about 6.4 Myrs at a metallicity of 0.001 (Schaller et al. 1992). This lifetime is more consistent with the most recent estimates for the end of the starburst; 10 Myrs would be too long ago.

The models yield an average  $T_{eff}$  in IC 4662 of somewhat hotter than about 45,000 K (log g=4.5 model) unless the H II regions are all Orion-like in size, which is unlikely. The  $L_{H\alpha}/L_{[OIII]}$  ratio yields a  $T_{eff}$  that is hotter than 45,000 K even if the ratio is larger by  $1\sigma$ . A  $T_{eff}$  of 45,000 K corresponds to an O4V star (Conti & Underhill 1988). The total H $\alpha$  luminosity of IC 4662, however, would correspond to only 50 equivalent O4V stars (or ~400 O6.5V stars). Thus, the total number of O stars in IC 4662 is significantly lower than in NGC 1569, but we are catching those regions at a much younger age unless the stellar initial mass function is highly top heavy which seems unlikely (Massey & Hunter 1998). The hydrogen-burning lifetime of an O4 star is about 3 Myrs (Schaller et al. 1992).

In both galaxies the average  $T_{eff}$  are hotter than what are usually determined for other galaxies. For example,  $T_{eff}$  determined from an [O III]88 measurement in the starburst nucleus of NGC 253 gives  $\geq 34,500$  K, which is equivalent to an O8.5V star (Carral et al. 1994). For a zero-age main sequence stellar population of the same stellar initial mass function, a higher  $T_{eff}$  could result if individual star-forming regions are richer in stars, rich enough to allow the rarer highest mass stars to form (Massey & Hunter 1998). In that case, then, we would expect to see supergiant H II regions associated with these large concentrations of massive stars or perhaps super star clusters. The luminosity function of H II regions in NGC 1569 does show that the H II region population in NGC 1569 extends to luminous H II regions ( $L_{H\alpha} \sim 10^{40}$  ergs s<sup>-1</sup>) (Youngblood & Hunter 1999; we do not have an H II region luminosity function for IC 4662), and NGC 1569 does contain two super star clusters. In addition, since NGC 1569 is a starburst system and, hence, the stellar population is coeval to a greater extent than in most galaxies, the average age of the O-star population is expected to be low compared to spirals with more continuous star formation.

# 5.1.3. $[OIII]\lambda 88$ and [CII]

The  $f_{[OIII]}/f_{[CII]}$  and  $f_{[OIII]}/f_{[OI]}$  ratios are much higher in the irregulars than they are in spirals. This is shown for  $f_{[OIII]}/f_{[CII]}$  in Figure 8. Plots of  $f_{[OIII]}/f_{[OI]}$  look similar to this since  $[O\,I]$  and  $[C\,II]$  both come mostly from PDRs. We see that the irregulars have  $f_{[OIII]}/f_{[CII]}$  ratios that are as much as 16 times higher than those in most spirals. We use the  $[N\,II]$  observations in §5.3.1 to show that most of the  $[C\,II]$  originates in PDRs as opposed to  $H\,II$  gas whereas  $[O\,III]$  comes from  $H\,II$  regions.

Even if there were no PDR contribution to the [C II] in irregulars, we would not expect differences of order 16 from spirals if the effective temperatures of the stars were not considerably higher in irregulars compared with spirals. In spirals, the H II regions contribute of order 0.2 to 0.5 of the [C II] emission (Malhotra et al 2001). Therefore, eliminating the PDR contribution would only increase the  $f_{[OIII]}/f_{[CII]}$  ratio by factors of 2-5 in spirals. The irregulars can only gain the large factor of 16 by also having less [C II] compared with [O III] in the H II region. This is accomplished by having higher effective temperature stars, which doubly ionize most species and leave only small quantities of  $C^+$  in the H II regions.

However, if H II regions in the irregulars in our sample were surrounded by optically thick PDRs ( $A_V > 1$ ), the  $f_{[OIII]}/f_{[CII]}$  ratio would be much smaller than observed, because such PDRs produce copious emission in [C II], quite independent of metallicity (Kaufman et al. 1999). Therefore, the extremely high ratios of  $f_{[OIII]}/f_{[CII]}$  observed in the irregulars in our sample can only be achieved by having both high effective temperature stars and small covering factors of optically thick PDRs outside the H II regions compared with normal spirals.

### 5.2. The PDR and Neutral Gas

Integrated  $L_{[CII]}/L_{CO}(1-0)$  ratios have been shown to be related to the global star formation activity of a galaxy (see, for example, Pierini et al. 1999). Stacey et al. (1991) have shown that galaxies with starburst nuclei have ratios comparable to those seen in Galactic star-forming regions, while more quiescent galactic nuclei have ratios that are about 3 times smaller and comparable to values averaged over entire Milky Way GMCs. Stacey et al. measured  $L_{[CII]}/L_{CO}$  values of 900–6100 for normal spirals and values of 1000–1800 for GMCs. By contrast Stacey et al. measured a ratio of 6100 for the starburst galaxy M82 and values of 5900–14000 for Milky Way H II regions. Poglitsch et al. (1995) measure a ratio of 60000 in the supergiant H II complex 30 Doradus, and Madden et al. (1997) find values of 1500–10000 throughout IC 10. Smith & Madden (1997) measured ratios of 14000 and 16000 for two Virgo spirals. There are, however, also variations among similar clouds. Israel et al. (1996) report variations of up to a factor of 100 among individual clouds in the LMC; they measured ratios of 400–34000 in 4 clouds, and attribute

the variations to evolutionary effects. At the other extreme, Malhotra et al. (2000) extend the  $L_{[CII]}/L_{CO}$  range to low values with ISO observations of early-type galaxies where presumably the environment is quite quiescent. Generally, regions of intense star formation, including kpc-sized regions in galaxies, have much higher  $L_{[CII]}/L_{CO}$  compared to more quiescent regions.

To place our irregular galaxies in this context, we have examined the  $L_{[CII]}/L_{CO}$  ratios for NGC 1156, NGC 1569, and IC 4662, and they are given in Table 4. The  $^{12}$ CO(1–0) observations are taken from Hunter & Sage (1993), Young et al. (1995), and Heydari-Malayeri et al. (1990), and  $L_{CO} = 0.119D^2S_{CO}$  from Kenney & Young (1989) where  $S_{CO}$  is the CO flux in Jy km s<sup>-1</sup> and D is the distance to the galaxy in Mpc. The lower limits on  $L_{[CII]}/L_{CO}$  for NGC 1156 and IC 4662 result from upper limits on  $L_{CO}$ . The observed ratios in the irregulars are very high: at least several times  $10^4$ . Galactic values of this level are also seen in the irregulars IC 10 (Madden et al. 1997) and the LMC (Mochizuki et al. 1994).

These values are much higher than values Stacey et al. (1991) and others measured for spiral nuclei and giant molecular clouds. But, they are also higher than values measured for all but one of the Milky Way H II regions and higher than that measured for the starburst galaxy M82. This can also be seen graphically in Figure 2(b) of Pierini et al. (1999) where they plot  $L_{[CII]}/L_{CO}$  against  $L_{[CII]}/L_{FIR}$ . All of the galaxies in their sample and our irregulars have similar  $L_{[CII]}/L_{FIR}$ , but our irregulars sit at higher  $L_{[CII]}/L_{CO}$  than all of the extragalactic and Galactic sources. The ratios for our three irregulars are not corrected for the smaller beam size of the CO observations, although the ratios of the beam sizes are given in Table 4, and in two cases the ratios are lower limits because of upper limits on the CO flux. Thus, the  $L_{[CII]}/L_{CO}$  ratios of these irregulars could be even higher.

Pierini et al. (1999) show that there is a correlation between  $L_{[CII]}/L_{CO}$  and  $H\alpha$  equivalent width in the sense that galaxies with high equivalent widths, indicating a higher relative star formation rate, have higher  $L_{[CII]}/L_{CO}$ . In our sample NGC 1569 has just undergone a starburst, and NGC 1156 and IC 4662 relatively high SFRs. In NGC 1569 the starburst has blown a hole in the H I (Israel & van Driel 1990) and severely disrupted the ISM. Yet in spite of this, NGC 1569's  $L_{[CII]}/L_{CO}$  ratio is of the same order of magnitude as that of the other two irregulars. Perhaps the five GMCs detected in NGC 1569 (Taylor et al. 1999) are dominating both the [C II] and CO emission.

The high  $L_{[CII]}/L_{CO}$  ratio in the irregulars could be an indication of a different geometry of clouds in irregulars compared to spirals (e.g., Pak et al. 1998, Kaufman et al. 1999, and references therein). If the PDR is a thin skin around a CO core, both the [CII] and CO luminosity from a cloud go as  $R^2$  and so the ratio is approximately constant for a dense warm PDR layer. However, if the CO core is small and the [CII] layer around the outside is very thick, the CO luminosity goes as  $R^2$  but the [CII] goes as  $(R+\Delta R)^2$  and the  $L_{[CII]}/L_{CO}$  ratio will be higher. Thus, Im galaxies could have very thick PDR regions around tiny molecular cores. This would also be consistent with the picture in which the molecular clouds are the dense cores of large, massive atomic gas

complexes (Rubio et al. 1991). In fact, below, we derive physical conditions of the PDRs from models, and find that for NGC 1569 the PDR is 6 pc thick, thicker than is usual in spirals.

It should also be kept in mind that  $L_{CO}$  in irregulars is probably an underestimate of the amount of molecular hydrogen that is present compared to the case in higher metallicity spirals. There is strong evidence that the conversion of  $I_{CO}$  to  $N(H_2)$  depends on the metallicity and that the CO component of a cloud in metal poor irregulars is a much smaller fraction of the  $H_2$  cloud (see, for example, Maloney & Black 1988; Dettmar & Heithausen 1989; Stacey 1993; Mochizuki et al. 1994; Poglitsch et al. 1995; Verter & Hodge 1995; Wilson 1995; Madden et al. 1997; Smith & Madden 1997; but see also Wilson & Reid 1991). In the LMC where the metallicity is about half solar, virial masses of molecular clouds yield a correction to the standard ratio of a factor of 6 (Cohen et al. 1988). A factor of 6.6 was also found for giant molecular clouds in NGC 1569 (Taylor et al. 1999), but the correction factor to  $L_{CO}$  remains somewhat controversial.

# 5.2.2. $[CII]\lambda 158$ and FIR Emission

Malhotra et al. (1997, 2001) report a correlation between integrated  $L_{[CII]}/L_{FIR}$  and  $f_{60}/f_{100}$  and  $L_{FIR}/L_B$  for the distant galaxy sample. The bulk of the galaxies have similiar  $L_{[CII]}/L_{FIR}$  ratios, but then as the FIR dust temperature increases, the  $L_{[CII]}/L_{FIR}$  ratio decreases and  $L_{FIR}/L_B$  increases. For most galaxies  $L_{[CII]}/L_{FIR}$  is about the same because  $G_0 \propto n^{1.4}$ . Here  $G_0$  is the far-ultraviolet (FUV) stellar radiation flux, in units of the value measured for the solar neighborhood, and n is the neutral gas density. Therefore,  $G_0/n$  rises slowly with  $G_0$ , which keeps the grain charge fixed and the gas heating efficiency via the grain and PAH photoelectric heating mechanism fixed. This implies similarities in star-forming clouds in different galaxies. Malhotra et al. (2001) interpret the decrease in  $L_{[CII]}/L_{FIR}$  at high values of  $f_{60}/f_{100}$  (FIR dust temperatures) in some galaxies as due to less efficient gas heating resulting from charged dust grains in high  $G_0/n$  regimes (Bakes & Tielens 1994). However, one should also question the normalization of  $L_{[CII]}/L_{FIR}$  given the role of PAHs (Helou et al. 2001).

Figure 9 shows the irregular galaxies in our sample relative to the spirals in  $L_{[CII]}/L_{FIR}$ . We see that NGC 1156 and a position in IC 10 have among the highest  $L_{[CII]}/L_{FIR}$  ratios of the entire sample of galaxies. The other two irregulars and other positions in IC 10 have  $L_{[CII]}/L_{FIR}$  ratios that are comparable to that of the bulk of the spirals. Furthermore, for a given FIR dust temperature, the irregular galaxies are seen to have a higher value of  $L_{[CII]}/L_{FIR}$  than irregulars.

For comparison, Israel et al. (1996) report a  $L_{[CII]}/L_{FIR}$  ratio of 0.01 for the supergiant H II complex 30 Doradus in the LMC and, presumably because it is dominated by 30 Doradus, for the LMC as a whole. The ratio observed in 30 Doradus is, therefore, 2–4 times higher than the integrated values for the irregulars in this sample. Even though NGC 1569 is a starburst galaxy, it is significantly lower in  $L_{[CII]}/L_{FIR}$  compared to a supergiant star-forming region, implying that average conditions in NGC 1569 today are not too extreme. This could mean that

the FIR emission in NGC 1569 is being dominated by the remaining GMCs and is not reflecting the disrupted nature of the rest of the ISM of the galaxy. The LMC, on the other hand, has a much higher integrated value of  $L_{[CII]}/L_{FIR}$  than NGC 1569 even though NGC 1569 has a recent SFR per unit area that is 30 times higher. This suggests that a supergiant H II region, when it is present, can dominate the integrated properties of a galaxy. We would predict, therefore, that NGC 2366 should have a  $L_{[CII]}/L_{FIR}$  ratio that is like that of the LMC since it is dominated by the supergiant H II complex NGC 2363. Unfortunately, we do not have LWS observations of NGC 2366.

The lower ratio of  $L_{[CII]}/L_{FIR}$  in spirals compared to our irregulars for the same  $f_{60}/f_{100}$ , might be an indication that cooler sources of radiation (than hot OB stars) may be contributing to the FIR luminosity in those sources with low  $L_{[CII]}/L_{FIR}$ . Another possibility is that the ratio of  $G_0/n$  is somewhat higher in those sources with low  $L_{[CII]}/L_{FIR}$ , resulting in more highly charged grains and less efficient gas heating.

In Figure 9 we also plot  $L_{[CII]}/L_{FIR}$  against the global SFR per unit area for the irregulars and other galaxies in the distant sample. We see that the bulk of the sample has a similar  $L_{[CII]}/L_{FIR}$  ratio with some decrease or more scatter of  $L_{[CII]}/L_{FIR}$  as the SFR per unit area decreases for the spirals (the irregulars appear to go counter to this trend, but the statistics are poor). This trend is similar to what is seen by Pierini et al. (1999) for a sample of Virgo cluster spirals, where they see a plateau value of 0.004 in  $L_{[CII]}/L_{FIR}$  and a drop to lower values for lower  $H\alpha$  equivalent widths. They suggest that this plateau is an average of compact and diffuse regions in the galaxy and that diffuse regions begin to dominate as the SFR declines. However, PDR models (Kaufman et al. 1999) and observations of diffuse regions in the Galaxy show that diffuse regions have lower  $G_0$ /n and, hence, higher  $L_{[CII]}/L_{FIR}$ . The near constancy with SFR means that a higher level of star formation in a given area does not imply a higher local  $G_0/n$ ratio. Although  $G_0$  goes up in regions of star formation, Malhotra et al. (2001) argue that n goes up too, so that ordinarily the average  $G_0/n$ , and hence  $L_{[CII]}/L_{FIR}$ , rises slowly. However, individual star-forming regions may have enhanced  $G_0/n$  ratios, which lead to inefficient heating by grains and lower  $L_{[CII]}/L_{FIR}$ . The large scatter for low values of SFR may be caused by a small number of star-forming regions dominating this regime, so that the local conditions in a particular star-forming region become more evident.

5.2.3. 
$$[OI]\lambda 145,63$$

The ratio  $f_{[OI]145}/f_{[OI]63}$  is a measure of the temperature of the gas or an indicator of optical depth in the 63  $\mu$ m line. Malhotra et al. (2001) interpret the increase of  $f_{[OI]145}/f_{[OI]63}$  with increasing  $L_{FIR}/L_B$  in the large sample of galaxies as an indication of optical depth effects in [OI]63. We have  $f_{[OI]145}/f_{[OI]63}$  for NGC 1569 and that measurement is shown in Figure 10. We see that NGC 1569 falls at the tail end of the relationship traced by the spirals. Thus, [OI]63 in NGC 1569 appears to be affected by optical depth as in spiral galaxies, but NGC 1569 lies at the

low optical depth end of the distribution.

## 5.3. Physical Conditions in the PDRs in Irregulars

The FIR emission-line ratios can be combined with PDR models in order to derive fundamental parameters that describe the state of the ISM in the irregular galaxies in our sample (Kaufman et al. 1999). In particular, the FIR line ratios yield information on the far-ultraviolet stellar radiation field,  $G_0$ , and the neutral gas density, n, of H nuclei in PDRs.

# 5.3.1. The PDR and H<sub>II</sub> Region Contributions to [C<sub>II</sub>]

A primary diagnostic is the [C II] line, but both PDRs and dense and diffuse H II regions can contribute to this line flux. In Figure 11 we plot the  $L_{[CII]}/L_{H\alpha}$  ratio against global  $L_{FIR}/L_B$ . The correlation of  $L_{[CII]}/L_{H\alpha}$  with  $L_{FIR}/L_B$  resembles that of  $f_{6.75}/f_{H\alpha}$  and  $f_{15}/f_{H\alpha}$  with  $L_{FIR}/L_B$  shown in Figure 5 although there is more scatter in the  $L_{[CII]}/L_{H\alpha}$  plot. As cold dust emission increases relative to the optical, the [C II], PAH, and small grain emissions all increase to some extent relative to H $\alpha$ . Thus, the amount of [C II] emission is related to the amount of cold dust emission, as expected. We see that the three irregulars in our sample have the lowest  $L_{[CII]}/L_{H\alpha}$  ratio of the distant galaxy sample. However, H II regions could be a significant source of [C II] emission, and that contribution needs to be removed in order to examine the emission from PDRs.

We have, therefore, determined corrections to  $L_{[CII]}$  for the H II contribution following the procedure of Malhotra et al. (2001). They used the fact that  $[N\,II]\lambda 122~\mu m$  emission comes only from the dense and diffuse ionized gas (not the PDR gas) and derive the ionized gas contribution to  $[C\,II]$  as 4.5 times the flux of  $[N\,II]$ . This correction factor assumes a C/N ratio of 1.9 and that may not be accurate for metal-poor irregulars. If irregular galaxies such as those for which we have LWS spectra have higher C/N ratios, as indicated by Garnett et al. (1995), the correction to  $[C\,II]$  would be correspondingly higher. On the other hand, for the three irregulars we only have upper limits to  $L_{[NII]}$  and hence lower limits to the PDR contribution to the  $[C\,II]$  flux,  $L_{[CII],PDR}$ . At least 61% of the  $[C\,II]$  emission in the irregulars is from PDRs. The  $L_{[OI]}/L_{[CII],PDR}$  ratios are given in Table 4 as a range of values with the lower end of the range determined assuming that all of  $[C\,II]$  comes from the PDRs and the upper end of the range determined assuming a correction to  $[C\,II]$  for H II regions that assumes the upper limit of the  $[N\,II]$  flux.

For IC 10 the contribution of ionized gas to [C II] was found to be  $\sim 20\%$  by Madden et al. (1997). Stacey et al. (1993) also found that 25%–30% of [C II] emission in the spirals NGC 6946 and NGC 891 comes from diffuse ionized gas, and Malhotra et al. (2001) find that the correction is typically 30%. Thus, unless we are underestimating the amount of [C II] coming from H II regions because of a different C/N ratio, at most the irregulars in our sample are similar to other galaxies in proportions of [C II] coming from PDR and ionized gas, and potentially our irregulars have a

somewhat lower proportion coming from ionized gas. This is a surprise because other parameters have led us to conclude that the integrated properties of irregular galaxies are dominated by H II regions more so than the spirals. However, because of the high effective temperature of the exciting stars, the H II regions in these irregulars will be in high ionization states, resulting in less C<sup>+</sup> in the H II gas than would otherwise be expected.

The ratios of [O I] to [C II] are shown in Figure 12 for the corrected and uncorrected [C II] flux. The points for the 3 irregulars are upper limits for  $L_{[OI]}/L_{[CII],PDR}$ , but those for two regions in IC 10 are measurements since the [N II] line was detected there. We see that our irregulars have  $L_{[OI]}/L_{[CII],PDR}$  ratios that are lower for a given  $f_{60}/f_{100}$  ratio compared to spirals.

### 5.3.2. Results from PDR Models

We have used the LWS line strengths in conjunction with models that are slightly modified from those presented by Kaufman et al. (1999). The analysis by Kaufman et al. is most appropriate for individual nearby molecular clouds where FUV illumination occurs primarily from one side of a molecular cloud. The models have been modified to consider integrated emission from a large fraction of a galaxy by assuming that the interstellar clouds can be illuminated from any side and that optically thin [C II] and FIR continuum reach the observer from any side. Because it is, however, optically thick, [O I] emission is assumed to come only from the side closest to the observer. The ratio  $(L_{[CII]}+L_{[OI]})/L_{TIR}$  measures the efficiency with which FUV photons are converted to emission lines. This is combined with the  $L_{[OI]}/L_{[CII],PDR}$  ratio to derive  $G_0$ , n, and the average gas surface temperature  $T_{gas}$  and pressure P of the interstellar gas producing the line and the FIR continuum in PDRs.

In this manner, we derive  $G_0$ , n,  $T_{gas}$ , and P given in Table 6 for PDRs in NGC 1156, NGC 1569, and IC 4662. We see that  $G_0$  is  $1.1 \times 10^3 - 2.4 \times 10^4$ , n is  $1.3 \times 10^3 - 2.8 \times 10^4$  cm<sup>-3</sup>, and  $T_{gas}$  is 310–725 K. The conditions in IC 4662 seem to be the most severe of the three irregulars.

For the larger group of spiral galaxies, Malhotra et al. (2001) derived  $G_0$  of  $10^2-10^{4.5}$  and n of  $10^2-10^{4.5}$  cm<sup>-3</sup>. A comparison of the irregulars with Figure 9 of Malhotra et al. (2001) shows how  $G_0$  in the irregulars compares with typical values in spirals: NGC 1156 has a  $G_0$  that is comparable to the bulk of spirals, IC 4662's  $G_0$  is higher than those of all but a few spirals, and NGC 1569 has a  $G_0$  that is higher than those of most of the spirals. The values of  $G_0$  and n derived for the irregulars, especially NGC 1569 and IC 4662, are similar to the values derived for the peculiar galaxy M82. For M82 Colbert et al. (1999) analyze LWS spectra to find that  $G_0$  is 630 and n is 2000 cm<sup>-3</sup>, but Kaufman et al. (1999) find a higher  $G_0$  of  $10^{3.5}$  and a higher n of  $10^4$  cm<sup>-3</sup> for the center of M82 from analysis of Kuiper Airborne Observatory data (Lord et al. 1996). Also, the central regions of IC 10, a galaxy that has many similarities to NGC 1569, have  $G_0$  that are a factor of 6 lower, 300–500, with densities that are similar,  $10^3-10^4$  cm<sup>-3</sup> (Madden et al. 1997). However, in the starburst nuclei of two spirals, Carral et al. (1994) measure  $G_0$ ,

 $10^3$ – $10^4$  that are similar to the three irregulars. Thus, the illuminated neutral clouds in irregulars are within the range of values observed for spiral galaxies but are at the high end, having a more intense stellar radiation field reaching the clouds and a higher density than most. Malhotra et al. interpret the high  $T_{gas}$  and P they derive for the spiral sample as indicating that most of the grain and gas heating is occurring very close to the concentrations of young, hot stars in these GMCs, and this must be the case in the irregulars as well.

We derive pressures P in the PDRs of  $4-200\times10^5$  K cm<sup>-3</sup>. Elmegreen & Hunter (2000) have estimated pressures of H II regions in a sample of 6 irregular galaxies (unfortunately, none of the galaxies are in common with our LWS observations). They find H II region pressures of  $10^4-10^5$  K cm<sup>-3</sup>. The pressures estimated from H II regions are therefore lower than those in the PDRs of our galaxies, although both pressure determinations are uncertain. The H II region pressures measured by Elmegreen and Hunter are lower probably because these regions are evolved enough that they no longer have PDRs around them.

The differences in physical PDR parameters between the irregulars NGC 1569 and IC 4662 and normal spiral galaxies imply that the star-forming clouds in NGC 1569 and IC 4662 are different. This is perhaps not a surprise since at least one of the galaxies is a starburst. NGC 1569 is a starburst galaxy with a high population of massive stars providing an intense FUV field, and the ISM has been disrupted in many ways. The very high  $G_0$  and n of IC 4662 suggest that maybe this galaxy has experienced some recent peculiar event like that of NGC 1569, these properties are also consistent with the higher average stellar  $T_{eff}$  found in §5.1.2. NGC 1156, on the other hand, is a normal, albeit active, irregular and its cloud properties are correspondingly more normal.

In order to further investigate the properties of the ISM in these three irregular galaxies, we use the technique of Wolfire, Tielens & Hollenbach (1990) along with the model results of Kaufman et al. (1999) modified for application to extragalactic sources. Given the PDR parameters derived from [O I], [C II] and FIR observations, the PDR models make specific predictions for the [C II] cooling rate per atom and the [C II] intensity. By comparing the cooling rate per atom with the observed [C II] flux from PDRs,  $L_{[CII],PDR}$ , an estimate of the atomic gas mass  $M_a$  in PDRs can be found. Following the measurements of Taylor et al. (1999) for NGC1569, we assume a carbon abundance of 1/6 solar, so  $x_C = 2.3 \times 10^{-5}$  in all three galaxies. From this, we find the mass of atomic gas on the outsides of molecular clouds in these three galaxies varies from  $\sim 1.3 \times 10^5 - 4 \times 10^7 \, M_{\odot}$ ; values are given in Table 6. An estimate of the area filling factor of PDR gas in a galaxy's central region producing [C II] emission can be made by comparing the observed [C II] intensity for this region with the predicted [C II] intensity from the PDR models. In order to make this comparison, we assume that the [C II] emitting region lies within the contours shown on the 6.75  $\mu$ m images in Figure 3 (see figure caption for H $\alpha$  surface brightness levels). Estimates of the PDR area filling factor range from  $\sim 6-10\%$  in the three galaxies.

To further extend the analysis, we need to find the mass of molecular gas in the clouds whose surfaces produce the PDR emission. NGC 1569 is the only galaxy of the three for which we have a measured value of the CO luminosity,  $L_{CO} = 35 L_{\odot}$ , from Young et al. (1995). The standard conversion factor,  $L_{CO}/M_{H_2} \sim 8 \times 10^{-6} L_{\odot}/M_{\odot}$  (e.g. Young et al. 1986) has been shown by Taylor et al. (1999) to be too large by a factor of  $\sim 6$  in this galaxy, reflecting a metallicity about 1/6 solar. By applying this correction to the standard conversion factor, we find a molecular gas mass M(H<sub>2</sub>) in NGC 1569 of  $1.9 \times 10^7 M_{\odot}$ , about 1.5 times the atomic gas mass. Values of M(H<sub>2</sub>) are given in Table 6.

A comparison of the surface area of the clouds (the [C II] measurement) with the volume of the clouds (the CO measurement) allows us to characterize the molecular clouds in NGC 1569, and the derived parameters are given in Table 7. If we assume that the [C II] and CO regions have equal density (that is,  $n(H_2)/n_a\sim 1$ ), then we find the emission is fit by an ensemble of 4 giant molecular clouds with typical radius  $\sim 25$  pc and cloud mass  $\sim 8\times 10^6 M_{\odot}$ . If, instead, we assume that the CO region has a density 3 times that of the atomic gas  $(n(H_2)/n_a\sim 3)$ , the number of clouds increases to 8, the mass per cloud decreases by a factor 2, and the cloud radius falls to 18 pc. These results for number of clouds and cloud size are similar to those of Taylor et al. (1999), who found from CO observations that the GMCs in NGC 1569 could be resolved into  $\sim 4-5$  clouds with radii  $\sim 20$  pc, though we note that they report cloud masses which are significantly lower than ours. Our clouds are  $\sim 20$  times more massive than a typical Milky Way GMC (Scoville & Sanders 1987).

The PDR surface layer on our clouds would extend  $\sim$ 6 pc in from the cloud surface, a distance larger than would be found if the clouds had solar metallicities. Given the derived density of the PDR gas,  $n=3.5\times10^3\,\mathrm{cm^{-3}}$ , these GMCs have a gas column density from surface to center of  $\sim3\times10^{23}\,\mathrm{cm^{-2}}$ , corresponding to a visual extinction of  $A_V\sim22$  assuming that dust is depleted by the same factor as the carbon. As a consistency check, we compare these results with those of Kaufman et al. (1999) who find that clouds with  $A_V\sim10$ ,  $n=10^3\,\mathrm{cm^{-3}}$ , and metallicities of a few tenths solar have L(CO)/M(H<sub>2</sub>) conversion factors of  $\sim10^{-6}L_{\odot}/M_{\odot}$ , very close to the corrected value of Taylor et al. (1999). The results for the NGC 1569 clouds give  $A_V$  higher by a factor of  $\sim3-4$  than the  $A_V$  predicted by the photoionization-regulated star formation model of McKee (1989). This may imply that the clouds in NGC 1569 have not yet reached equilibrium, which may be consistent with the disruption of the ISM from the recent starburst and the proximity of the GMCs to the super star clusters (Taylor et al. 1999). (Note that these high extinction values only apply to the GMCs which are not necessarily visible in the optical).

One thing that is clear from these observations is that the PDR observations in irregulars are sensitive, not to the average density of GMCs, but to the conditions in the denser clumps within the GMCs. In the Milky Way, the average GMC density is of order 100 cm<sup>-3</sup>, but observations of FUV illuminated gas give PDR densities of order 10<sup>3</sup> cm<sup>-3</sup> and higher. Such is the case, for example, in Orion where the average density of the entire molecular cloud complex is far lower than that in the FUV illuminated clumps region at the edge of the Orion Nebula.

A similar analysis to the one carried out above may be done for the other two galaxies, NGC

1156 and IC 4662. However, in both cases we only have upper limits to the molecular mass. As a result, we can only derive ranges for the numbers and masses of GMCs in these galaxies with large uncertainties. In NCG 1156, we find between 1 and 6 GMCs with masses ranging from  $\sim 7 \times 10^7$  M<sub> $\odot$ </sub> to  $3 \times 10^8$  M<sub> $\odot$ </sub>; for IC 4662, we find between 1 and 2 GMCs with masses from  $\sim 3 \times 10^6$  M<sub> $\odot$ </sub> to  $8 \times 10^6$  M<sub> $\odot$ </sub>. These GMCs are also large compared to those in the Milky Way (Scoville & Sanders 1987): 175–750 times more massive in NGC 1156 and 7–20 times in IC 4662.

### 5.3.3. Uncertainties in PDR Modelling

To quantify the uncertainties in deriving  $G_0$  and n, we have used several different methods for each galaxy. In the PDR models, we typically compare one line ratio (usually,  $L_{[CII]}/L_{[OI]}$ ) with the infrared line-to-continuum ratio, ( $L_{[OI]+[CII]}/L_{TIR}$ ). If we do this using the raw [O I], [C II] and FIR values, we get certain values for  $G_0$  and n, but we suspect that much of the [C II] emission comes from ionized gas, not PDRs. Thus, we correct [C II] to get [C II]\_{PDR}. The correction is based on the observed [N II] flux with the assumption that [N II] only comes from ionized gas; given an assumed [C II]-to-[N II] abundance ratio, we can calculate the [C II] from ionized gas and subtract that portion from the total [C II], leaving only the PDR contribution. In all three galaxies, we assumed that the C/N ratio was 4.6. However, for all three galaxies we only have upper limits on the [N II] flux, so we have a range of possible [C II] from PDRs. In one variation on the standard method, if one assumes that there is no [N II], then all of the [C II] comes from PDRs, and the models give significantly different answers for  $G_0$  and n. A second variation is to solve for  $G_0$  and n using other ratios. In this case, we compared  $L_{[OI]}/L_{FIR}$  with  $L_{60}/L_{100}$ . This has the advantage that we no longer rely on the [C II] measurements, though we do have to assume that the 60 and 100 micron fluxes are produced in PDRs. Again, we get somewhat different results for  $G_0$  and n.

In Figure 13, we summarize the results of the three methods. These three methods together give an estimate of the uncertainty in the model values of  $G_0$  and n and hence clouds masses and sizes. One can see that the three methods give answers that can be uncertain by up to an order of magnitude in  $G_0$  and n. These uncertainties almost surely are larger than the uncertainties in the measurements. What is heartening is that the preferred method gives results within a factor  $\sim 3$  of the other two methods.

### 6. Summary and Comments

We have discussed mid-infrared imaging and FIR spectroscopy of a sample of 5 IBm galaxies observed by *ISO* as part of a larger study of galaxies of all Hubble types. The galaxies include NGC 1156, NGC 1569, NGC 2366, NGC 6822, and IC 4662. The galaxies NGC 1156, NGC 1569, and IC 4662 are high luminosity, high surface brightness, and high star formation rate systems relative to median properties of larger samples of irregulars, and so are not typical irregulars.

NGC 2366 is dominated by a supergiant H<sub>II</sub> complex, and NGC 6822, although more of a typical irregular, yielded useful data with CAM.

The mid-infrared imaging of all 5 galaxies is in two bands: one at 6.75  $\mu$ m that is dominated by PAHs and one at 15  $\mu$ m that is dominated by small dust grains. The spectroscopy of 3 of the galaxies (NGC 1156, NGC 1569, and IC 4662) includes [C II] $\lambda$ 158  $\mu$ m and [O I] $\lambda$ 63  $\mu$ m, important coolants of PDRs, and [O III] $\lambda$ 88  $\mu$ m and [N II] $\lambda$ 122  $\mu$ m, that come from ionized gas regions. [O I] $\lambda$ 145  $\mu$ m and [O III] $\lambda$ 52  $\mu$ m were measured in NGC 1569 as well. We compare the observations of the irregulars with the larger sample of spiral galaxies observed as part of our *ISO* program.

### We observe the following:

- In the mid-infrared images most of the emission we detect is associated with the brightest H II regions in the galaxies, and the integrated  $f_{6.75}/f_{15}$  ratios are comparable to what is observed in regions of star formation.
- The ratio of PAH-to-small grain emission drops as the FIR color temperature becomes hotter in all galaxies, and the irregulars in our sample lie mostly at the warmer  $f_{60}/f_{100}$  and lower  $f_{6.75}/f_{15}$  end of the distribution.
- The ratio of PAH-to-FIR emission drops as the FIR color temperature becomes hotter while the small grain emission-to-FIR ratio remains more nearly constant in all galaxy types.
- The irregular galaxies in our sample have low PAH emission at 6.75  $\mu$ m and low small grain emission at 15  $\mu$ m relative to H $\alpha$  emission, compared to spirals. The f<sub>6.75</sub>/f<sub>H $\alpha$ </sub> ratio drops with increasing FIR color temperature, while the f<sub>15</sub>/f<sub>H $\alpha$ </sub> ratio is constant among our irregulars.
- The PAH and small grain emissions relative to  $H\alpha$  both increase as  $L_{FIR}/L_B$  increases for all galaxies, possibly with a plateau in the value of  $f_{15}/f_{H\alpha}$  for low values of  $L_{FIR}/L_B$ . Our irregular galaxies lie at the low  $L_{FIR}/L_B$  end of the distributions.
- The [C II] emission is higher relative to FIR emission in these irregulars than in spirals of the same FIR color temperature. The [C II] line represents 0.3% to 1% of the FIR emission of the irregulars.
- The [C II] emission in our irregulars is high relative to the PAH 6.75 μm emission compared to spirals, and f<sub>[CII]</sub>/f<sub>6.75</sub> is constant among the irregulars. On the other hand, for small grains, the f<sub>[CII]</sub>/f<sub>15</sub> ratio drops as the FIR color temperature increases for all galaxies, but the f<sub>[CII]</sub>/f<sub>15</sub> ratio is high in the irregulars compared to spirals with the same FIR color temperature.
- For our irregulars the ratio of [O III] to [C II] is very high compared to spirals. In addition, the high [C II] to 6.75  $\mu$ m and FIR emissions suggest that [O III] is high relative to the infrared continuum and other lines as well.

- For all galaxies the  $f_{[CII]}/f_{H\alpha}$  ratio increases as  $L_{FIR}/L_B$  increases, and our irregulars are at the low  $f_{[CII]}/f_{H\alpha}$ , low  $L_{FIR}/L_B$  end of the distribution.
- In the irregulars in our sample the [O III] emission is high with respect to [C II].
- The  $L_{[CII]}/L_{CO}$  ratio is very high among our sample of irregulars.
- From PDR models we derive physical conditions in the PDRs of NGC 1156, NGC 1569, and IC 4662: Radiation fields relative to the solar neighborhood  $G_0$  are  $10^{3.0}$ – $10^{4.4}$ , gas densities n are  $10^{3.1}$ – $10^{4.4}$  cm<sup>-3</sup>, and pressures P are  $10^{5.6}$ – $10^{7.3}$  cm<sup>-3</sup> K. In NGC 1569, where  $L_{CO}$  has been measured, we deduce the presence of 4 GMCs with masses of that are about 20 times higher than that of a typical GMC in the Milky Way, and the PDR is 6 pc thick.

The upper limits on the  $[N\,II]\lambda 122~\mu m$  emission in our irregulars indicate that a large fraction of the  $[C\,II]$  emission detected in these irregulars comes from PDR gas and the component from H II regions is small although these conclusions do depend on physical conditions being similar to spirals. Less than 39% of the  $[C\,II]$  originates from H II regions. In spite of the high  $[O\,III]$  and  $H\alpha$  emission relative to  $[C\,II]$ , the contribution of ionized gas regions to  $[C\,II]$  emission is similar to or less than the fractions observed for spirals.

The average stellar effective temperatures in NGC 1569 and IC 4662 are high compared to measurements in other galaxies. In NGC 1569 this is consistent with the presence of two young super star clusters and luminous H II regions, and suggests an end to the recent starburst of  $\leq 6$  Myrs ago. This result is also consistent with the measurement of exceptionally high  $f_{[OIII]}/f_{[CII]}$  ratios in our irregulars. The high excitation stars ionize most of the H II regions to higher ionization states, reducing the amount of [C II] in H II regions. Our irregulars also have higher  $L_{[CII]}/L_{FIR}$  ratios for their FIR color temperatures relative to spirals. This can be understood if the spirals have a larger contribution to heating of the dust from cooler stars, presumbably from the general interstellar radiation field, than do the irregulars.

The increase in  $f_{6.75}/f_{H\alpha}$  and  $f_{15}/f_{H\alpha}$  with increasing  $L_{FIR}/L_B$  tells us that the PAH and small grain emissions are related to the total dust emission. However, the decrease in PAH emission in the irregulars in our sample relative to small grain, FIR, and  $H\alpha$  emissions for increasing FIR color temperature is interpreted as a decrease in PAH emission resulting from an increase in the radiation field due to star formation, either through destruction of the PAH itself or of the 6.75  $\mu$ m carrier on the PAH.

That the  $f_{15}/f_{H\alpha}$  ratio is constant among the irregulars that we observed means that the more hot stars that are formed, the more small grains are heated. The 15  $\mu$ m emission may come primarily from small grains in H II regions. We interpret the linear dependence of the 15  $\mu$ m flux with H $\alpha$  to mean that the 15  $\mu$ m emission is being generated by the transient heating of small dust grains by single photon events, possibly Ly $\alpha$  photons trapped in H II regions. The low  $f_{15}/f_{H\alpha}$  ratio, as well as the high  $f_{[CII]}/f_{15}$  ratio, in our irregulars compared to spirals may be due to the

lower dust content overall resulting in dust grains being, on average, further away from the heating source. By contrast, it has been suggested that the 15  $\mu$ m emission in spirals may be warm dust grains radiating on the Wien side of the blackbody spectrum rather than transient single photon events. This interpretation is consistent with the increase in  $f_{15}/f_{H\alpha}$  ratio with hotter FIR color temperature seen in spirals, but not irregulars.

The high [C II] emission relative to FIR, PAH emission at 6.75  $\mu$ m, and small grain emission at 15  $\mu$ m in our irregulars is harder to interpret. The small scatter in the f<sub>[CII]</sub>/f<sub>6.75</sub> ratio among spirals has been interpreted as meaning that the PAHs that produce the 6.75  $\mu$ m emission and the PAHs that heat the PDR and hence produce the [C II] emission are the same entities. But, then the much higher f<sub>[CII]</sub>/f<sub>6.75</sub> ratio in our irregulars compared to spirals would require that the PAHs in irregulars produce several times more heat than the PAHs in spirals. Alternatively, the small scatter in f<sub>[CII]</sub>/f<sub>6.75</sub> among spirals could be explained if the carrier of the 6.75  $\mu$ m feature tracks the heating but contributes only a part of the heating, which is due mostly to small grains or other PAHs. In this scenario these irregulars are understood if they have a higher proportion of the PAHs that heat the PDRs to the PAHs that produce the 6.75  $\mu$ m feature. A different incident spectral energy distribution could also play a role.

Our data give some clues to the geometry of the clouds in the irregulars in our sample. The high  $[O\,III]/[C\,II]$  ratio requires a small solid angle of optically thick  $(A_V>1)$  PDRs outside the H II regions. That is, if the H II region is surrounded by an optically thick PDR, the copious production of  $[C\,II]$  there would lower the  $f_{[O\,III]}/f_{[C\,II]}$  ratio. So, the optically thick component of the PDR must present a smaller covering factor in our irregulars compared to spirals. This picture is also consistent with the fact that PAH 6.75  $\mu$ m and  $[C\,II]$  emissions, both of which come primarily from PDR gas, are lower compared to H $\alpha$ . On the other hand, the  $L_{[C\,II]}/L_{CO}$  ratio is very high among our sample of irregulars, higher than values measured in spirals or H II regions. A picture in which the clouds in our irregulars have very thick  $[C\,II]$  shells around tiny CO cores compared to clouds in spirals is consistent with physical parameters we derive for NGC 1569's PDRs.

From models we deduce the physical conditions in the PDRs. The FUV stellar radiation field  $G_0$  is like that in typical spirals in NGC 1156 but much higher in the starburst galaxy NGC 1569 and in IC 4662. That NGC 1569 stands out in  $G_0$  makes sense since it is a starburst system. We emphasize, however, that the conditions measured by the data presented here apply to very local conditions in star-forming clouds, particularly the denser clumps within GMCs. That is why NGC 1569, in fact, does not appear far more extreme than it does.

Finally, we estimated the number of molecular clouds, their masses, and their sizes within the LWS beam in NGC 1156, NGC 1569, and IC 4662. We deduce the presence of a few clouds in each galaxy with masses much larger than typical Milky Way GMCs. These extraordinarily large clouds may also be necessary to form super star clusters, as NGC 1569 has recently done.

The irregular galaxies in our sample have star formation rates normalized to their size that

are comparable to those in spirals. In fact, the star formation rates span the entire range observed in our spiral sample, including the high end of the range. However, the infrared properties of the irregulars are dominated by star-formation, perhaps more than is the case in spirals. This implies that the ISM beyond the H II regions and associated PDRs in irregulars is too faint to contribute measureably to the *ISO* observations. We know that the ISM in irregulars can be quite clumpy and that ionizing photons can travel large distances. But, the low contribution of the ISM beyond H II regions to the infrared may be a consequence of a lower stellar radiation field outside star-forming regions and reflect the general low surface brightness disk of irregulars. In galaxies with low dust column densities, without concentrations of hot stars to heat the dust and gas, the ISM becomes very hard to detect in PAH, small grain, and PDR emission features.

What does this imply about more normal irregulars? Most of the irregular galaxies in our sample are not representative of typical irregular galaxies. Several in our sample are very high surface brightness and one is a starburst. Most irregulars are lower in surface brightness and star formation activity. Unfortunately, we were not able to observe these galaxies with *ISO*. However, it is likely that more typical irregulars, if they could be observed, would also turn out to be dominated by star-forming regions since these would be the primary contributors to the FIR and mid-infrared emission. The irregulars can be seen as containing glowing islands of star-forming regions in a sea of otherwise relatively dim gas and stars.

We are grateful to P. Massey and C. Claver for the use of their optical images. This work was supported in part by ISO data analysis funding from the US National Aeronautics and Space Administration through the Jet Propulsion Laboratory (JPL) of the California Institute of Technology and in part by support to D.A.H. from the Lowell Research Fund and grant AST-9802193 from the National Science Foundation. The H $\alpha$  imaging would not have been possible without filters purchased through funds provided by a Small Research Grant from the American Astronomical Society, National Science Foundation grant AST-9022046, and grant 960355 from JPL. D.A.H. wishes to thank Lowell Observatory for the observing time on the Perkins 1.8 m telescope that produced the northern H $\alpha$  images and optical long-slit spectroscopy.

### REFERENCES

- Aparicio, A., Cepa, J., Gallart, C., Castañeda, H. O., Chiosi, C., Bertelli, G., Mas-Hesse, J. M., Muñoz-Tuñón, C., Telles, E., Tenorio-Tagle, G., Diaz, A. I., García-Vargas, L. M., Garzón, F., González-Delgado, R. M., Pérez, E., Rodríguez-Espinosa, J. M., Terlevich, E., & Televich, R. J. 1995, AJ, 110, 212
- Arp, H., & Sandage, A. 1985, AJ, 90, 1163
- Bakes, E. L. O., & Tielens, A. G. G. M. 1994, ApJ, 427, 822
- Bolatto, A. D., Jackson, J. M., Wilson, C. D., Moriarty-Schieven, G. 2000, ApJ, 532, 909
- Boselli, A., et al. 1997, A&A, 324, L13
- Burstein, D., & Heiles, C. 1984, ApJS, 54, 33
- Cardelli, J. A., Clayton, G. C., & Mathis, J. S. 1989, ApJ, 345, 245
- Carral, P., Hollenbach, D. J., Lord, S. D., Colgan, S. W. J., Haas, M. R., Rubin, R. H., & Erickson, E. F. 1994, ApJ, 423, 223
- Cesarsky, C. J., et al. 1996a, A&A, 315, L32
- Cesarsky, D., Lequeux, J., Abergel, A., Perault, M., Palazzi, E., Madden, S., & Tran, D. 1996b, A&A, 315, L305
- Cesarsky, D., Lequeux, J., Abergel, A., Perault, M., Palazzi, E., Madden, S., & Tran, D. 1996c, A&A, 315, L309
- Clegg, P. E., et al. 1996, A&A, 315, L38
- Cohen, J. G., & Blakeslee, J. P. 1998, AJ, 115, 2356
- Cohen, R. S., Dame, T. M., Garay, G., Montani, J., Rubio, M., & Thaddeus, P. 1988, ApJ, 331, L95
- Colbert, J. W., et al. 1999, ApJ, 511, 721
- Conti, P. S., & Underhill, A. B. 1988, O Stars and Wolf-Rayet Stars, NASA SP-497 (Washington, D.C., NASA)
- Contursi, A., Lequeux, J., Hanus, M., Heydari-Malayeri, M., Bonoli, C., Bosma, A., Boulanger, F., Cesarsky, D., Madden, S., Sauvage, M., Tran, D., & Vigroux, L. 1998, A&A, 336, 662
- Dale, D. A., Helou, G., Silbermann, N. A., Contursi, A., Malhotra, S., & Rubin, R. H. 1999, AJ, 118, 2055
- Dale, D. A., Silbermann, N. A., Brauher, J., Helou, G., Malhotra, S., Valjavec, E., Beichman, C.
  A., Contursi, A., Dinerstein, H., Hollenbach, D., Hunter, D., Kolhatkar, S., Lo, K. Y., Lord,
  S., Lu, N. Y., Rubin, R., Stacey, G., Thronson, H. Jr., & Werner, M. 2000, AJ, 120, 583
- Dale, D. A., Helou, G., Contursi, A., Silbermann, N. A., Kolhatkar, S. 2001, ApJ, in press

de Vaucouleurs, G., de Vaucouleurs, A., Corwin, H., Buta, R., Paturel, G., & Fouqué, P. 1991, Third Reference Catalogue of Bright Galaxies (New York, Springer-Verlag) (RC3)

de Vaucouleurs, G., de Vaucouleurs, A., & Pence, W. 1974, ApJ, 194, L119

Dettmar, R.-J., & Heithausen, A. 1989, ApJ, 344, L61

Drissen, L., Roy, J.-R., Robert, C., Devost, D., & Doyon, R. 2000, AJ, 119, 688

Elmegreen, B. G., & Hunter, D. A. 2000, ApJ, submitted

Gallagher, J. S. III, Hunter, D. A., Gillett, F. C., & Rice, W. L. 1991, ApJ, 371, 142

Gallagher, J. S., Hunter, D. A., & Tutukov, A. V. 1984, ApJ, 284, 544

Gallart, C., Aparicio, A., Bertelli, G., & Chiosi, C. 1996b, AJ, 112, 1950

Gallart, C., Aparicio, A., Bertelli, G., & Chiosi, C. 1996c, AJ, 112, 2596

Gallart, C., Aparicio, A., Chiosi, C., Bertelli, G., & Vilchez, J. M. 1994, ApJ, 425, L9

Gallart, C., Aparicio, A., & Vilchez, J. M. 1996a, AJ, 112, 1928

Garnett, D. R. 1990, ApJ, 363, 142

Garnett, D. R., Skillman, E. D., Dufour, R. J., Peimbert, M., Torres-Peimbert, S., Terlevich, R., Terlevich, E., & Shields, G. A. 1995, ApJ, 443, 64

Giard, M., Lamarre, J. M., Pajot, F., & Serra, G. 1994, A&A, 286, 203

Greggio, L., Tosi, M., Clampin, M., & De Marchi, G. 1998, ApJ, 504, 725

Helou, G. 2001, in The Extragalactic Infrared Background and its Cosmological Implications, IAU Symposium #204, in press

Helou, G., Khan, I., Malek, L., Boehmer, L. 1988, ApJS, 68, 151

Helou, G., Malhotra, S., Beichman, C. A., Dinerstein, H., Hollenbach, D. J., Hunter, D. A., Lo, K. Y., Lord, S. D., Lu, Y. Y., Rubin, R. H., Stacey, G. J., Thronson, H. A. Jr., & Werner, M. W. 1996, A&A, 315, L157.

Helou, G., Malhotra, S., Hollenbach, D. J., Dale, D. A., & Contursi, A. 2001, ApJL, in press

Heydari-Malayeri, M., Melnick, J., & Martin, J.-M. 1990, A&A, 234, 99

Hodge, P. W. 1977, ApJS, 33, 69

Hodge, P., Kennicutt, R. C. Jr., & Lee, M. G. 1988, PASP, 100, 917

Hodge, P., Smith, T., Eskridge, P., MacGillivray, H., & Beard, S. 1991, ApJ, 379, 621

Hoessel, J. G., & Anderson, N. 1986, ApJS, 60, 507

Hollenbach, D. J., Takahashi, T., & Tielens, A. G. G. M. 1991, ApJ, 377, 192

Huchtmeier, W. K. 1979, A&A, 75, 170

Hudgins, D. M., Allamandola, L. J., & Sanford, S. A. 1997, AdSpR, 19, 999

Hunter, D. A. 1997, PASP, 109, 937

Hunter, D. A., & Gallagher, J. S. 1985, ApJS, 58, 533

Hunter, D. A., & Gallagher, J. S. 1986, PASP, 98, 5

Hunter, D. A., & Gallagher, J. S. 1990, ApJ, 362, 480

Hunter, D. A., & Gallagher, J. S. 1992, ApJ, 391, L9

Hunter, D. A., & Gallagher, J. S. 1997, ApJ, 475, 65

Hunter, D. A., & Gallagher, J. S., & Rautenkranz, D. 1982, ApJS, 49, 53

Hunter, D. A., Gallagher, J. S., Rice, W. L., & Gillett, F. C. 1989, ApJ, 336, 152

Hunter, D. A., Hawley, W. N., & Gallagher, J. S. 1993, AJ, 106, 1797

Hunter, D. A., & Hoffman, L. 1999, AJ, 117, 2789

Hunter, D. A., & Sage, L. 1993, PASP, 105, 374

Israel, F. P., Maloney, P. R., Geis, N., Herrmann, F., Madden, S. C., Poglitsch, A., & Stacey, G. J. 1996, ApJ, 465, 738

Israel, F. P., & van Driel, W. 1990, A&A, 236 323

Karachentsev, K., Musella, I., & Grimaldi, A. 1996, A&A, 310, 722

Kaufman, M. J., Wolfire, M. G., Hollenbach, D. J., & Luhman, M. L. 1999, ApJ, 527, 795

Kayser, S. E. 1967, AJ, 72, 134

Kenney, J. D., & Young, J. S. 1989, ApJ, 344, 171

Kennicutt, R. C. 1983, ApJ, 272, 54

Kennicutt, R. C., & Hodge, P. W. 1986, ApJ, 300, 132

Kessler, M. F., Steinz, J. A., Anderegg, M. E., Clavel, J., Drechsel, G., Estaria, P., Faelker, J., Riedinger, J. R., Robson, A., Taylor, B. G., & Ximenez De Ferran, S. 1996, A&A, 315, L27

Killen, R. M., & Dufour, R. J. 1982, PASP, 94, 444

Kobulnicky, H. A., & Skillman, E. D. 1997, ApJ, 489, 636

Lord, S. D., Hollenbach, D. J., Haas, M. R., Rubin, R. H., Colgan, S. W., J., & Erickson, E. F. 1996, ApJ, 465, 703

Lord, S., et al. 2000, in preparation

Lu, N. Y., et al. 2000, in preparation

Madden, S. C., Poglitsch, A., Geis, N., Stacey, G. J., & Townes, C. H. 1997, ApJ, 483, 200

Malhotra, S., et al. 1997, ApJ, 491, L27

Malhotra, S., Hollenbach, D., Helou, G., Silbermann, N., Viljavec, E., Dale, D., Hunter, D., Lu, N., Lord, S., Dinerstein, H., & Thronson, H. 2000, ApJ, 543, 634

Malhotra, S., Kaufman, M. J., Hollenbach, D., Helou, G., Rubin, R. H., Brauher, J., Dale, D., Lu, N. Y., Lord, S., Stacey, G., Contursi, A., Hunter, D. A., & Dinerstein, H. 2001, ApJ, in press

Maloney, P., & Black, J. H. 1988, ApJ, 325, 389

Marconi, G., Tosi, M., Greggio, L., & Focardi, P. 1995, AJ, 109, 173

Massey, P., & Armandroff, T. E. 1995, AJ, 109, 2470

Massey, P., Armandroff, T. E., Pyke, R., Patel, K., & Wilson, C. D. 1995, AJ, 110, 2715

Massey, P., & Hunter, D. A. 1998, ApJ, 493, 180

Massey, P., & Johnson, O. 1998, ApJ, 505, 793

McAlary, C. W., Madore, B. F., & Davis, L. E. 1984, ApJ, 276, 487

McKee, C. F. 1989, ApJ, 345, 782

Melisse, J. P. M., & Israel, F. P. 1994, A&AS, 103, 391

Mochizuki, K., Makagawa, T., Doi, Y., Yui, Y. Y., Okuda, H., Shibai, H., Yui, M., Nishimura, T., & Low, F. J. 1994, ApJ, 430, L37

O'Connell, R. W., Gallagher, J. S., & Hunter, D. A. 1994, ApJ, 433, 63

Pak, S., Jaffe, D. T., van Dishoeck, E. F., Johansson, L. E. B., & Booth, R. S. 1998, ApJ, 498, 735

Panagia, N. 1973, AJ, 78, 929

Pastoriza, M. G., & Dottori, H. A. 1981, ApJ, 244, 27

Pierini, D., Leech, K. J., Tuffs, R. J., & Völk, H. J. 1999, MNRAS, 303, L29

Poglitsch, A., Krabbe, A., Madden, S. C., Nikola, T., Geis, N., Johansson, L. E. B., Stacey, G. J., & Sternberg, A. 1995, ApJ, 454, 293

Rice, W., Lonsdale, C. J., Soifer, B. T., Neugebauer, G., Kpan, E. L., Lloyd, L. A., de Jong, T., & Habing, H. J. 1988, ApJS, 68, 91

Rubin, R. H. 1985, ApJS, 57, 349

Rubin, R. H., Simpson, J. P., Lord, S. D., Colgan, S. W. J., Erickson, E. F., & Haas, M. R. 1994, ApJ, 420, 772

Rubio, M., Garay, G., Montani, J., & Thaddeus, P. 1991, ApJ, 368, 173

Saito, M., Sasaki, M., Ohta, K., & Yamada, T. 1992, PASJ, 44, 593

Salpeter, E. 1955, ApJ, 121, 161

Schaller, G., Schaerer, D., Meynet, G., & Maeder, A. 1992, A&AS, 96, 269

Scoville, N. Z., & Sanders, D. B. 1987, in Interstellar Processes, ed D. J. Hollenbach and H. A. Thronson (Dordrecht: Reidel), p 21

Smith, B. J., & Madden, S. C. 1997, AJ, 114, 138

Stacey, G. J. 1993, in Astronomical Infrared Spectroscopy: Future Observational Directions, ed. Sun Kwok (San Francisco:Astronomical Society of the Pacific), p 297

Stacey, G. J., Geis, N., Genzel, R., Lugten, J. B., Poglitsch, A., Sternberg, A., & Townes, C. H. 1991, ApJ, 373, 423

Stil, J. M., & Israel, F. P. 1998, A&A, 337, 64

Talent, D. L. 1980, PhD thesis, Rice University

Taylor, C. L., Hüttemeister, S., Klein, U., & Greve, A. 1999, A&A, 349, 424

Tolstoy, E., Saha, A., Hoessel, J. G., & McQuade, K. 1995, AJ, 110, 1640

Vallenari, A., & Bomans, D. J. 1996, A&A, 313, 713

Wilcots, E. M., & Miller, B. W. 1998, ApJ, 116, 2363

Wilson, C. D. 1995, ApJ, 448, L97

Wilson, C. D., & Reid, I. N. 1991, ApJ, 366, L11

Verter, F., & Hodge, P. 1995, ApJ, 446, 616

Young, J. S., Xie, S., Tacconi, L., Knezek, P., Viscuso, P., Tacconi-Garman, L., Scoville, N., Schneider, S., Schloerb, F. P., Lord, S., Lesser, A., Kenney, J., Huang, Y.-L., Devereux, N., Claussen, M., Case, J., Carpenter, J., Berry, M., & Allen, L. 1995, ApJS, 98, 219

This preprint was prepared with the AAS LATEX macros v4.0.

- Fig. 1.—  $\mathrm{H}\alpha$  images of the galaxies in our sample shown with V-band contours superposed. The stellar continuum has been subtracted from the H $\alpha$  images. The stars have been removed from the V-band images as well for NGC 1156 and NGC 2366, and the V-band images of NGC 2366 and NGC 6822 were smoothed before contouring. The V-band images of NGC 1156, NGC 1569, and NGC 2366 are courtesy of P. Massey, and the V-band image of NGC 6822 is courtesy of C. Claver. The image of IC 4662 shows a region, labeled IC 4662-A, that is well separated from the main body of the galaxy (890 pc at IC 4662). It has the H $\alpha$  luminosity of a large OB association. Three tiny H II regions between IC 4662 and IC 4662-A have H $\alpha$  luminosities similar to that of the Orion nebula. One arcminute corresponds to 2.3 kpc at NGC 1156, 0.7 kpc at NGC 1569, 1.0 kpc at NGC 2366, 0.14 kpc at NGC 6822, and 0.6 kpc at IC 4662.
- Fig. 2.— Spectra of FIR emission lines observed with ISO. The y-axes are in units of  $10^{-14}$  W cm<sup>-2</sup>  $\mu$ m<sup>-1</sup>. The spectra of IC 4662 include two observations of each line. The two observations differ markedly in the continuum levels due to calibration uncertainties in the dark current subtraction.
- Fig. 3.— Mid-infrared CAM images of the irregular galaxies. The LW2 filter was centered at 6.75  $\mu$ m. Objects labeled "star" are foreground stars, and the object in NGC 2366 labeled "Gal" is a background galaxy (Drissen et al. 2000). Contours are of H $\alpha$  emission where the H $\alpha$  images have been transformed to the geometry of the CAM images and pixel scale. Named H II regions are labeled in NGC 2366 and NGC 6822 (Hodge 1977, Killen & Dufour 1982). In the image of NGC 1569, the four plus signs mark the positions of the 5 giant molecular clouds mapped by Taylor et al. (1999), where two of the clouds are given as one position, and the two five-pointed stars mark the positions of the super star clusters. One arcminute corresponds to 2.3 kpc at NGC 1156, 0.7 kpc at NGC 1569, 1.0 kpc at NGC 2366, 0.14 kpc at NGC 6822, and 0.6 kpc at IC 4662. H $\alpha$  contours, in units of  $10^{34}$  ergs s<sup>-1</sup> arcsec<sup>-2</sup>, are 7.8 and 46.9 for NGC 1156; 1.1, 5.4, and 42.8 for NGC 1569; 0.2, 1.4, and 6.6 for NGC 2366;  $3.1 \times 10^3$  for NGC 6822; and 0.2, 0.4, 0.6, 2.4, and 11.4 for IC 4662.
- Fig. 4.— Mid-infrared ratio  $f_{6.75}/f_{15}$  plotted against the FIR ratio  $f_{60}/f_{100}$  and the area-normalized star formation rate (SFR). The dashed line marks a  $f_{6.75}/f_{15}$  of 1. The area used to normalize the star formation rate is  $\pi R_{25}^2$ .
- Fig. 5.— Ratio of mid-infrared flux to H $\alpha$  flux for LW2 (PAH-dominated) and LW3 (small dust grain dominated). This is plotted against the FIR ratio  $f_{60}/f_{100}$  and the ratio of the integrated FIR flux to the B-band flux. The  $L_{H\alpha}$  have been corrected for reddening.
- Fig. 6.— Ratio of mid-infrared flux to FIR flux for LW2 (PAH-dominated) and LW3 (small dust grain dominated). This is plotted against the FIR color ratio  $f_{60}/f_{100}$ .
- Fig. 7.— Ratio of  $[C II]\lambda 158~\mu m$  emission to mid-infrared LW2 and LW3 emission. These are plotted against the FIR ratio  $f_{60}/f_{100}$  and the ratio of the integrated FIR to the B-band flux of the galaxy. The  $f_{6.75}$  and  $f_{15}$  are in units of ergs cm<sup>-2</sup> s<sup>-1</sup> Hz<sup>-1</sup> and the units of [C II] are ergs cm<sup>-2</sup> s<sup>-1</sup>, so the ratios have units of Hz<sup>-1</sup>.

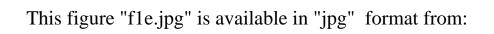
- Fig. 8.— Ratio of  $[O III]\lambda 88 \mu m$  to [C II] emission plotted against  $f_{60}/f_{100}$ .
- Fig. 9.— Ratio of  $L_{[CII]}/L_{FIR}$  plotted against the  $f_{60}/f_{100}$  and star formation rate per unit area. Data for the LMC comes from Israel et al. (1996), Kennicutt & Hodge (1986), RC3, and Rice et al. (1988).
- Fig. 10.— Ratio of  $[OI]\lambda 145 \mu m$  to  $[OI]\lambda 63 \mu m$  versus  $L_{FIR}/L_B$  for spirals in the distant galaxy sample (dots) and for the irregular NGC 1569 (star).
- Fig. 11.— Ratio of  $[C_{II}]\lambda 158~\mu m$  to  $L_{H\alpha}$  plotted against the  $L_{FIR}/L_B$  ratio.  $L_{H\alpha}$  has been corrected for reddening.
- Fig. 12.— Ratio of  $[O\ I]\lambda63\ \mu m$  to  $[C\ II]\lambda158\ \mu m$  plotted against the FIR color. In the top panel  $[C\ II]$  is the total measured. In the bottom panel an estimate of the contribution of H II regions to  $[C\ II]$  has been subtracted to leave only emission from PDRs. For the three irregulars NGC 1156, NGC 1569, and IC 4662 the corrections assume the full value of upper limits. For IC 10 and the distant galaxy sample the corrections were determined from  $[N\ II]\lambda122\ \mu m$  as described by Kaufman et al. (1999).
- Fig. 13.— Derived values of  $G_0$  and n for the three irregular galaxies NGC 1156, NGC 1569 and IC 4662. Squares show the values of  $G_0$  and n determined using uncorrected values of the [C II] intensity in the comparison of  $L_{[OI]}/L_{[CII]}$  with  $L_{[OI]+[CII]}/L_{TIR}$ ; triangles show the values determined when the value of [C II] corrected for the H II region contribution is used in the same comparison; and pentagons show the values determined when  $L_{[OI]}/L_{TIR}$  is compared with the IRAS  $f_{60}/f_{100}$  ratio. The third method is independent of the [C II] correction (see text). The results from these three methods give the reader a feel for the uncertainties in the modelling of PDR properties.

This figure "f1a.jpg" is available in "jpg" format from:

This figure "f1b.jpg" is available in "jpg" format from: http://arxiv.org/ps/astro-ph/0012354v1

This figure "f1c.jpg" is available in "jpg" format from:

This figure "fld.jpg" is available in "jpg" format from:



This figure "f2a.jpg" is available in "jpg" format from:

This figure "f2b.jpg" is available in "jpg" format from:

This figure "f2c.jpg" is available in "jpg" format from:

This figure "f3a.jpg" is available in "jpg" format from:

This figure "f3b.jpg" is available in "jpg" format from:

This figure "f3c.jpg" is available in "jpg" format from:

This figure "f3d.jpg" is available in "jpg" format from:

This figure "f3e.jpg" is available in "jpg" format from:

This figure "f4.jpg" is available in "jpg" format from:

This figure "f5.jpg" is available in "jpg" format from:

This figure "f6.jpg" is available in "jpg" format from:

This figure "f7.jpg" is available in "jpg" format from:

This figure "f8.jpg" is available in "jpg" format from:

This figure "f9.jpg" is available in "jpg" format from:

TABLE 1 BASIC GALAXY DATA.

Galaxy	Alternate Name	D <sup>a</sup> (Mpc)	${ m M}_B{}^{ m b}$	$ m R_{25}^{\ c}$ $ m (kpc)$	$E(B-V)_f^d$	$E(B-V)_g^e$	$\mu_{25}{}^{\mathrm{f}}$	$\log L_{H\alpha}^{g}$ (erg s <sup>-1</sup> )	$\frac{\log}{\mathrm{SFR/area^h}}$	12+ log(O/H) <sup>i</sup>
NGC 1156	PGC 11329 UGC 2455	7.8	-18.03	3.8	0.17	0.40	22.43	40.81	-1.99	8.39
NGC 1569	PGC 15345 UGC 3056 Arp 210 VIIZw16	2.5	-17.44	1.3	0.51	0.70	20.29	40.83	-1.06	8.17
NGC 2366	PGC 21102 UGC 3851 DDO 42	3.4	-16.61	4.0	0.03	0.03	23.35	40.12	-2.71	8.32
NGC 6822	PGC 63616 IC 4895 DDO 209 Barnard's Galaxy	0.5	-15.28	1.1	0.22	0.54	22.74	39.60	-2.17	8.27
IC 4662	PGC 60851	2.0	-14.77	0.8	0.07	0.09	22.10	39.76	-1.39	8.06

<sup>&</sup>lt;sup>a</sup>Distance to NGC 6822 is taken from McAlary et al. (1983; see also Kayser [1967] and Gallart, Aparicio, & Vílchez [1996a]); to IC 4662 from Heydari-Malayeri et al. (1990); to NGC 1569 from O'Connell, Gallagher, & Hunter (1994); to NGC 1156 from Karachentsev et al. (1996); and to NGC 2366 from Tolstoy et al. (1995).

 $<sup>^{\</sup>mathrm{b}}$ Determined from  $\mathrm{B}_{T}$  taken from RC3, corrected for reddening using the foreground reddening plus 0.05 mag internal reddening and the reddening law of Cardelli et al. (1989).

 $<sup>^{</sup>m c}$ From RC3. The radius of the galaxy at a B-band surface brightness of 25 mag arcsec $^{-2}$ .

<sup>&</sup>lt;sup>d</sup>Foreground reddening, determined from Burstein & Heiles (1984).

eTotal nebular reddening determined from emission spectra of HII regions. Taken from Hunter & Hoffman (1999), Talent (1980), and Heydari-Malayeri et al. (1990).

<sup>&</sup>lt;sup>f</sup>B-band surface brightness within  $R_{25}$ . From RC3, corrected for reddening, in units of magnitudes arcsec<sup>-2</sup>. <sup>g</sup>Measured from calibrated Hα images for NGC 1156, NGC 2366, and IC 4662; taken from Gallagher et al. (1991) for NGC 6822. Corrected for reddening. Uncertainties in  $L_{H\alpha}$  are of order 10%.

hStar formation rate per unit area in units of  $M_{\odot}$  yr<sup>-1</sup> kpc<sup>-2</sup>. Determined from  $L_{H\alpha}$  and the formula of Hunter & Gallagher (1986) that uses a Salpeter (1955) stellar initial mass function integrated from 0.1 to 100  ${\rm M}_{\odot}$ . The area is that contained in  ${\rm R}_{25}$ .

<sup>&</sup>lt;sup>i</sup>Oxygen abundances measured from H II regions. From Hunter & Hoffman (1999), Talent (1980), Heydari-Malayeri et al. (1990), Kobulnicky & Skillman (1997), and Garnett (1990).

TABLE 2

ISO OBSERVATIONS.

Galaxy	CAM	LWS Lines Observed	LWS Position <sup>b</sup> RA,DEC
NGC 1156 NGC 1569	LW2,LW3 LW2,LW3	[OI] $\lambda$ 63 $\mu$ m, [NII] $\lambda$ 122 $\mu$ m, [CII] $\lambda$ 158 $\mu$ m [OI] $\lambda$ 63 $\mu$ m, [OIII] $\lambda$ 88 $\mu$ m, [NII] $\lambda$ 122 $\mu$ m, [CII] $\lambda$ 158 $\mu$ m [OIII] $\lambda$ 52 $\mu$ m, [NIII] $\lambda$ 57 $\mu$ m, [OI] $\lambda$ 145 $\mu$ m	$02^h 59^m 42.5^s, +25^{\circ} 14' 15'' $ $04^h 30^m 49.0^s, +64^{\circ} 50' 53''$
NGC 2366 NGC 6822 IC 4662	LW2,LW3 LW2,LW3 LW2,LW3	$[{\rm OI}]\lambda 63~\mu{\rm m,}~[{\rm OIII}]\lambda 88~\mu{\rm m,}~[{\rm NII}]\lambda 122~\mu{\rm m,}~[{\rm CII}]\lambda 158~\mu{\rm m}$	$17^h \ 47^m \ 06.4^s, \ -64^{\circ} \ 38' \ 25''$

<sup>&</sup>lt;sup>a</sup>CAM was the mid-infrared camera. The LW2 filter in CAM was centered at 6.75  $\mu$ m with a  $\Delta\lambda$  of 3.5  $\mu$ m; LW3 was centered at 15  $\mu$ m with  $\Delta\lambda$  6.0  $\mu$ m. LWS was the long-wavelength spectrograph. <sup>b</sup>J2000.

 $\begin{tabular}{ll} TABLE~3\\ MID-INFRARED~FLUXES~AND~RATIOS^a. \end{tabular}$ 

01: 4	f <sub>6.75</sub>	$f_{15}$	c /c	1 c /c h	1 c /c b
Object	(Jy)	(Jy)	$f_{6.75}/f_{15}$	$\log f_{6.75}/f_{H\alpha}^{b}$	$\log f_{15}/f_{H\alpha}^{b}$
Integrated Gal	axies:				
$\widetilde{NGC}$ 1156	0.088	0.141	0.62	-13.00	-12.81
	0.018	0.028	0.18	0.20	0.20
NGC 1569	0.319	1.427	0.22	-13.45	-12.80
	0.060	0.290	0.06	0.19	0.20
NGC 2366	0.017	0.173	0.10	-13.77	-12.76
	0.003	0.035	0.03	0.18	0.20
NGC 6822	0.097	0.308	0.31	-14.14	-13.63
	0.019	0.062	0.09	0.19	0.20
IC 4662	0.050	0.164	0.30	-13.38	-12.86
	0.010	0.033	0.09	0.20	0.20
HII Regions:					
NGC 1156-N	0.017	0.072	0.24	-11.60	-10.97
	0.003	0.014	0.07	0.18	0.19
NGC 1156-S	0.014	0.021	0.65	-11.54	-11.36
	0.003	0.004	0.18	0.20	0.19
NGC 2363	0.013	0.180	0.08	-13.73	-12.60
	0.003	0.040	0.02	0.21	0.21
Hubble X	0.014	0.039	0.35	-14.48	-14.03
	0.003	0.008	0.10	0.20	0.20
Hubble V	0.043	0.190	0.23	-14.05	-13.40
	0.009	0.038	0.07	0.20	0.20
KD 11	0.010	0.037	0.27	-13.46	-12.89
	0.002	0.007	0.08	0.20	0.19
Ho 8	0.016	0.026	0.62	-13.36	-13.15
	0.003	0.005	0.18	0.19	0.19

<sup>&</sup>lt;sup>a</sup>Each entry is followed by a line containing the uncertainties. Flux uncertainties in CAM data are dominated by calibration uncertainties and are taken to be 20%. Uncertainties in the ratios with H $\alpha$  are assumed to add 0.1 to the uncertainty of the logarithm.

<sup>&</sup>lt;sup>b</sup>f<sub>6.75</sub> and f<sub>15</sub> are in units of Jy=  $10^{-23}$  ergs cm<sup>-2</sup> s<sup>-1</sup> Hz<sup>-1</sup>, while f<sub>H $\alpha$ </sub> are in units of erg cm<sup>-2</sup> s<sup>-1</sup>. So, the ratio has units of Hz<sup>-1</sup>.

TABLE 4
LINE FLUXES AND RATIOS<sup>a</sup>

Quantity	NGC 1156	NGC 1569	IC 4662
$f_{[OIII]\lambda52}^{\mathrm{b}}$		1.853	
		0.104	
$f_{[NIII]\lambda57}^{b}$		$\leq 0.206$	
$f_{[NIII]\lambda57}^{b}$ $f_{[OI]\lambda63}^{b}$	0.082	0.659	0.145
	0.006	0.051	0.011
$f_{[OIII]\lambda 88}^{b}$		2.768	0.458
		0.091	0.017
$f_{[NII]\lambda122}^{b}\dots\dots$ $f_{[OI]\lambda145}^{b}\dots\dots$	< 0.0084	< 0.0319	< 0.0107
$f_{[OI]\lambda145}^{b}$		0.0134	
		0.0025	
$f_{[CII]\lambda158}^{bb$	0.156	0.599	0.125
	0.010	0.020	0.006
$L_{[CII]}/L_{FIR}^{c}$	0.0051	0.0025	0.0027
_	0.0012	0.0004	0.0001
$L_{[CII]}/L_{H\alpha}^{d}$	0.18	0.07	0.06
	0.02	0.00	0.00
$L_{H\alpha}(LWS beam)/L_{H\alpha}(total)$	0.70	0.76	0.79
$L_{[CII]}/L_{CO}^{e}$	>10000	37000	> 34000
CO beam area/LWS beam area	0.64	0.36	0.33
$\log f_{[CII]}/f_{6.75}^{f} \dots \dots$	12.25	12.27	12.40
	0.09	0.08	0.09
$\log f_{[CII]}/f_{15}^{f}$	12.04	11.62	11.88
	0.09	0.09	0.09
$f_{[OIII]\lambda52}/f_{[OIII]\lambda88}$	• • • •	0.67	• • •
. 2	• • •	0.04	• • •
$n_e  (\mathrm{cm}^{-3})  \dots $	• • •	<300	
$f_{[OIII]\lambda 88}/f_{[CII]}$	• • •	4.61	3.66
0 10		0.18	0.23
$f_{[OI]\lambda63}/f_{[OI]\lambda145}$	• • •	49.2	• • •
T /T		9.9	
$L_{[OI]\lambda63}/L_{[CII]}$	0.39	1.10	1.16
T /T	0.22	0.08	0.07
$L_{[CII],PDR}/L_{[CII]}$	$\geq 0.76$	$\geq 0.76$	$\geq 0.61$
$L_{[OI]\lambda63}/L_{[CII],PDR}^{g}$	0.53 – 0.69	1.10 - 1.44	1.16 - 1.89

TABLE 4—Continued

Quantity	NGC 1156	NGC 1569	IC 4662
$L_{H\alpha}/L_{[OIII]\lambda88}^{h}$		2.48 0.46	$2.07 \\ 0.40$

<sup>a</sup>Second, unlabelled line contains the uncertainties in the

values in the first line.  $^{\rm b}$ Units of  $10^{-18}$  W cm<sup>-2</sup>.  $^{\rm c}$ The far-infrared luminosity is the global galactic value, not just that contained within the LWS aperture.

<sup>d</sup>The H $\alpha$  luminosity is the global galactic value.

eThe CO fluxes are not corrected for the differing beam size compared to the LWS aperture. The ratio of the beam sizes is given in the next line. CO upper limits are taken from Hunter & Sage (1993) and Heydari-Malayeri et al. (1990), assuming a line width of 20 km  $\rm s^{-1}$  and a conversion factor of 34 to go from K km s<sup>-1</sup> to Jy km s<sup>-1</sup>. The CO value for NGC 1569 is from Young et al. (1995) without their deconvolution with an exponential disk model. Conversion to  $L_{CO}$  uses the formula of Kenney & Young (1989),

that uses a Galactic-derived conversion factor.  $^{\rm f}f_{6.75}$  and  $f_{15}$  are in units of ergs cm $^{-2}$  s $^{-1}$  Hz $^{-1}$  and the units of [CII] are ergs cm $^{-2}$  s $^{-1}$ , so the ratio has units of

Hz<sup>-1</sup>.

gThe lower end of the range corresponds to no correction for the [CII] emission; the upper end corresponds to the total amount of the upper limit of the correction given above.

 ${}^{\rm h}{\rm L}_{H\alpha}$  is the H $\alpha$  luminosity in the LWS beam.

TABLE 5Integrated IRAS Fluxes<sup>a</sup>

Galaxy	$f_{12}$ (Jy)	$f_{25}$ (Jy)	$f_{60}$ (Jy)	$f_{100}$ (Jy)	$f_{12}/f_{25}$	$f_{60}/f_{100}$	$(10^{-17}  \mathrm{W  cm^{-2}})$	$(10^{40} \text{ ergs s}^{-1})$	$\mathcal{L}_{FIR}/\mathcal{L}_{B}{}^{\mathrm{b}}$	${ m L}_{TIR}/{ m L}_{FIR}{}^{ m c}$
NGC 1156	0.17	0.55	5.24	10.48	0.31	0.50	3.02	220	0.38	2.1
	0.05	0.08	0.90	2.40	0.12	0.18	0.59		0.08	
NGC 1569	1.23	8.79	54.25	55.36	0.14	0.98	24.61	185	0.56	1.9
	0.10	1.10	7.00	8.00	0.02	0.18	3.30		0.07	
NGC 2366	0.21	1.05	4.10	4.34	0.20	0.94	1.88	26	0.18	1.9
	0.04	0.08	0.60	0.70	0.04	0.21	0.28		0.03	
NGC 6822	0.84	6.46	58.86	130.80	0.13	0.45	35.61	11	0.23	2.2
	0.04	0.39	8.79	29.51	0.02	0.06	6.57		0.04	
IC 4662	0.30	1.25	9.27	12.65	0.24	0.73	4.61	22	0.50	1.9
	0.03	0.03	0.04	0.11	0.02	0.01	0.02		0.00	

 $<sup>^{\</sup>rm a}$  IRAS fluxes have been reextracted from the database. Original fluxes were from Hunter et al. (1989), Rice et al. (1988), and Sanders et al. (1995). The subscripts 12, 25, 60, and 100 refer to the flux in the 12  $\mu \rm m$ , 25  $\mu \rm m$ , 60  $\mu \rm m$ , and 100  $\mu \rm m$  passbands, respectively. Second line for each galaxy gives the uncertainties of the values given in the first line. The uncertainties for NGC 6822 were assumed to be 15%.  $^{\rm b} \rm L_B$  are monochromatic luminosities determined from  $f_{\nu}(\rm B)$  times the central frequency of the B-passband.  $^{\rm c} \rm TIR$  is the total infrared luminosity form 2–1100  $\mu \rm m$ .

 $\begin{array}{c} \text{TABLE 6} \\ \text{PDR MODEL RESULTS.} \end{array}$ 

Galaxy	$G_0{}^{\mathrm{a}}$	$n_a [\mathrm{cm}^{-3}]^{\mathrm{a}}$	$T_{gas}[K]$	$P[\mathrm{cm}^{-3} \mathrm{~K}]$	${\rm M}_a[{\rm M}_\odot]$	$\mathrm{M}(\mathrm{H}_2)[\mathrm{M}_{\odot}]$
NGC 1156	$3.2 \times 10^{3}$	$1.3 \times 10^{3}$	310	$4.0 \times 10^5$	$4.0 \times 10^{7}$	$< 1.8 \times 10^8$
NGC 1569		$3.5 \times 10^{3}$	375	$1.3 \times 10^6$	$1.3 \times 10^{7}$	$1.9 \times 10^7$
IC 4662		$2.8 \times 10^{4}$	725	$2.0 \times 10^7$	$1.3 \times 10^{5}$	$< 8.5 \times 10^6$

<sup>&</sup>lt;sup>a</sup>Properties derived by comparing PDR models of Kaufman et al. (1999) with observed emission ratios  $L_{[CII],PDR}/L_{[OI]}$  and  $(L_{[CII],PDR}+L_{[OI]})/L_{FIR}$ .

 $\begin{array}{c} \text{TABLE 7} \\ \text{Cloud Properties in NGC 1569}. \end{array}$ 

$n(\mathrm{H}_2)/n_a$	$N_{ m clouds}$	$R_{\rm cloud}[{ m pc}]$	$\rm M_{\rm cloud}[M_{\odot}]$	$A_V$
1	4	25	$7.8 \times 10^6$ $4.0 \times 10^6$	22
3	8	18		35

This figure "f10.jpg" is available in "jpg" format from:

This figure "f11.jpg" is available in "jpg" format from:

This figure "f12.jpg" is available in "jpg" format from:

This figure "f13.jpg" is available in "jpg" format from: